Design and Evaluation of an Automated Fiber Optic Untwisting Machine
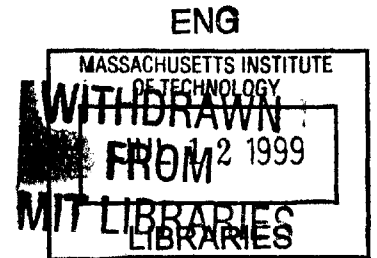
by

Pankaj B. Lad

B.S. Mechanical Engineering
The University of Texas at Austin, 1997

Submitted to the Department of Mechanical Engineering
in Partial Fulfillment of the Requirements for the Degree of
Master of Science in Mechanical Engineering

at the

Massachusetts Institute of Technology

June 1999

Signature of Author ....

Department of Mechanical Engineering
May 19, 1999

Approved by...

Peter Wender
Principal member of technical staff, Draper Laboratory
Technical Supervisor

Certified by ....

Dr. Andre Sharon
Director of the MIT Manufacturing Institute
Thesis Supervisor

Accepted by...

Ain A. Sonin
Chairman, Department Committee on Graduate Students

Design and Evaluation of an Automated Fiber Optic Untwisting Machine

by

Pankaj B. Lad

Abstract

Fiber optic gyroscopes (FOG's) offer much higher reliability for inertial guidance as compared to conventional mechanical gyroscopes. Unfortunately, the manufacturability of high performance FOGs has been limited by a laborious fiber coil winding process. In recent years, the development of automated coil winding equipment has allowed larger throughputs of these difficult to manufacture coils. Even with automated equipment, flaws during the winding process are inevitable. In the past, coil manufacturers have relied on increasing fiber tension to enforce proper winding position; however, higher tension tends to degrade a coil's performance.

Twisted fiber is one cause of flaws during the winding process. The elastic twist prevents the fiber from lying in a desired location. Instead, the fiber has a tendency to roll into a non-ideal gap or climb position that generates winding errors. As a solution, this author's thesis documents the conception of a fiber untwisting process that was embodied in a fully automated demonstration machine. Details of the design and construction of this machine are documented as well as preliminary untwisting results. As a recommendation for future work, this thesis discusses modifications to the untwisting machine that will enable it to address another gyro error source, drift caused by the Faraday effect.

Thesis Supervisor: Dr. Andre Sharon
Title: Director of the MIT Manufacturing Institute

Technical Supervisor: Peter Wender
Title: Principal member of technical staff, Draper Laboratory

PERSONAL ACKNOWLEDGMENTS

Dr. Andre Sharon, for introducing me to the dynamic world of research. These past two years have taught me in unexpectedly diverse areas, which allows me to depart MIT with much more than a SM degree. I thank you for this opportunity to join the ranks of MIT alumni.

Peter Wender, for reminding me that patience is a researcher's greatest tool. I highly respect your ability to be an excellent mentor and a professional role model.

Draper Laboratory, for giving me an opportunity to work with one of world's premier R&D facility.

Brian Surette, I am deeply indebted to you. I have learned a great amount from your many years of experience as a machinist.

Min Tsai, for your incredible love for the coil winder. I envy you.

Tang Yew Tan, for providing valuable peer support and constantly questioning the meaning of life. We made it buddy!

Jason Melvin, for expanding my engineering abilities. You've shown our lab what true fashion is really about!

Sieu Tru Duong, for keeping a sense of mystery in the air. The lab remembers you every time someone needs some spare change.

Jamie, Amir, and Fardad, for keeping me entertained with "lively" discussions.

Kara Meredith, for helping me with the dirty work.

Bruno, Betty, and Ralph, for being there when my machine misbehaved.

Draper and LMP machine shops, for the excellent advice and resources.

Wayne Hsiao, for showing me a different perspective on life. I hope to see your Alfa running one day.

David Chargin, for letting me sound off my joys and fears about my project. You've definitely added another dimension to my MIT experience.

Sameer, for giving brotherly advice that kept me sane. I will always cherish our years as roommates at both UT and here at MIT.

My family, for the love and support that has given me a set of wings allowing me to soar to new heights and higher achievements.
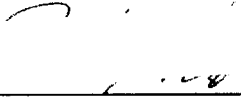
ACKNOWLEDGMENT

May 19, 1999

Permission is hereby granted by the Author to the Massachusetts Institute of Technology to reproduce any or all of this thesis.

_____   _____
                                   (author's signature)

TABLE OF CONTENTS

TABLE OF FIGURES

TABLE OF TABLES

CHAPTER 1 INTRODUCTION

Explorers would return from their journeys with recordings of rivers, mountains, and other geographical features so others could repeat their expeditions. This marked the beginning of navigation. As they moved seaward, coastal features like lighthouses kept sailors orientated near the shore, but pathfinding quickly became challenging in the far seas. In the 15th century, celestial navigation was combined with magnetic compasses, which allowed sailors to make longer and farther voyages. Determining longitude was feasible in the 18th century with the advent of an accurate timekeeper, the spring escapement chronometer. A huge leap in navigation occurred in 1852 when Jean-Bernard-Léon Foucault invented the first mechanical gyroscope, a device that ushered in the possibility of inertial navigation [1].

1.1. Mechanical Gyroscopes

Until about 1980, all navigation gyroscopes had been mechanical devices that measure rate of rotation in inertial space. The operation of mechanical gyros is based on the conservation of momentum of a spinning mass. Applying an input rotation about an axis normal to the mass spin vector causes the spin to precess about the remaining orthogonal axis [2]. In normal mechanization, some external action is taken to restore the precession angle to zero, and that action is proportional to the input rate. The action might be the rotation of an external support gimbal or the application of a precession-axis counter torque [3], [4].

In either case the mechanization, especially for highly accurate operation, is not only complex but requires the use of many parts [5]. Though great effort has been expended to cost-reduce these parts, the parts are still difficult to manufacture and remain an impediment to cost-reducing mechanical gyros. In addition, the electronics and sensors in the gyros add expense due to their high accuracy and low noise requirements [6].

Another drawback of mechanical gyros is that they contain moving parts that are subject to failure over time. For example, a bearing may wear out, or a part of the structure may fatigue and fail. In these cases, the gyroscope would become useless and would have to be replaced. On vehicles such as satellites, this is not easy and could render the satellite useless. If moving parts could be eliminated altogether, these problems could be avoided [6].

1.2. Optical Gyroscopes

Optical solid state technology has been shown in the last few years to be a viable substitute to the traditional mechanical technology used in gyroscopes. These solid state gyros incorporate few moving parts, relying on light traveling through an optical pathway to detect rotation. There are several ways that the optical pathway can be created. Ring Laser Gyros (RLGs) and Fiber Optic Gyros (FOGs) use two of the possible methods. As suggested by its name, the RLG is a laser that uses a set of accurate mirrors arranged in a closed circuit around which the light can travel. The FOG uses optical fiber to define the light path. The RLG is in volume production for many applications, but for cost reasons, the FOG seems to be the more promising future alternative [7].

FOGs approach the precision of current mechanical gyros and can operate under equal, or even harsher environmental conditions. The drawback to date has been the expense of developing and building high performance versions of these solid state gyros. Only recently has the state of technology begun to progress enough to bring the cost of manufacturing the gyros down to competitive levels. Optical fiber has become less expensive and methods of interfacing the fiber with other components in the gyro have improved due to advances in the telecommunications industry. Likewise, solid state light sources for the sensor have recently become far more affordable [6].

1.3. Theory of a Fiber Optic Gyroscope

The basic theory behind the FOG is fairly simple. Consider a long strand of optical fiber that is wrapped into a coil. The fiber is wound such that the two fiber ends are located on the outside of the coil as shown in the Figure 1.1. Two optical signals, generated by splitting a common source and therefore having the same phase, are launched into both ends of the fiber coil. If the coil remains stationary, the signals will have identical transit times and will exit in phase. However, if the coil rotates about its axis, as indicated in Figure 1.1, light traveling through the coil in the direction of the rotation will take longer to travel the fiber length than the light traveling against the direction of rotation [8]. This phenomenon is known as the Sagnac effect.
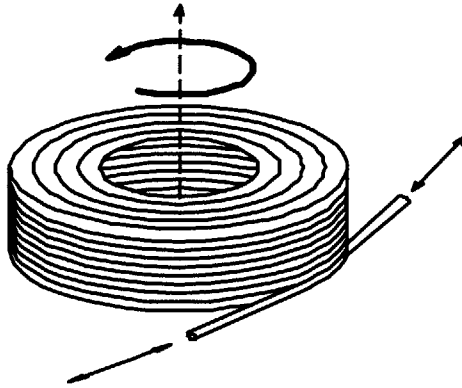
Figure 1.1. A representation of a FOG coil [6].

Figures 1.2 and 1.3 show a simple kinematic analogy to illustrate the Sagnac

effect. Assume that wave packets A and B travel at identical velocities along the

perimeter of the disk. In the first case (Figure 1.2) where the disk is stationary, both

particles will reach the starting point at the same time and experience no difference in

path length.

(a)   (b)
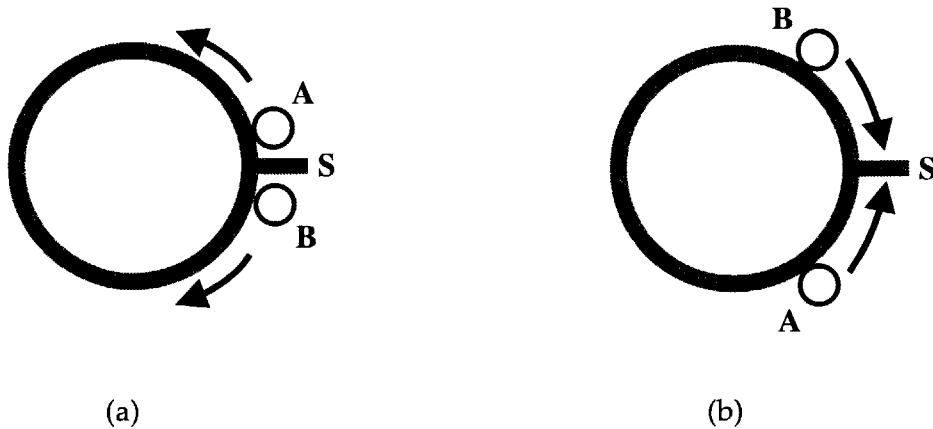
Figure 1.2. Since the disk does not rotate (a), both packets,
A and B, will reach point S at the same moment (b).

In a second case (Figure 1.3), the disk rotates at an angular velocity of Ω in a counterclockwise direction. Einstein reminds us that the propagation velocity of light in a medium is independent of the velocity of the medium. Therefore, packets A and B still travel at identical velocities; however, their velocities relative to the disk are now different. In this case, packet B appears to travel faster than packet A, but in actuality, point S has rotated by some angle. This creates different path lengths. The relationship between the path length difference, ΔL, of the two light beams and the rate of rotation, Ω, for a single-loop path is given by Equation 1.1 [9].

(a)   (b)
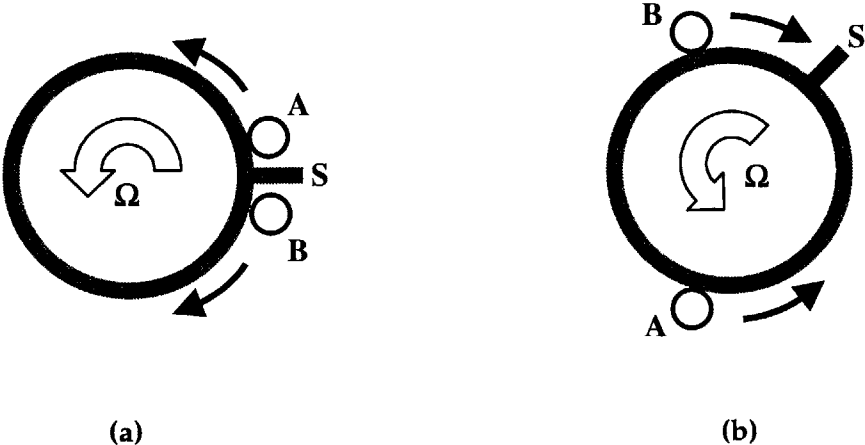
Figure 1.3. Disk rotates with some angular velocity, Ω (a).
Packet B has greater relative velocity than packet A;
therefore, packet B reaches point S first (b).

$$\Delta L = \frac{4A}{c} \Omega \qquad \qquad \textbf{Equation 1.1}$$

where A = area enclosed by the path
           c = velocity of light in a vacuum
           Ω = rotation rate
          ΔL = path length difference

In an optical domain, the path length difference will result in a phase shift. In FOGs, a light beam of a known frequency is split and enters the fiber optic loop. If the loop is rotating, the light waves will exit the loop with a path length difference and thus be out of phase. A single optical loop of a FOG gives a phase shift of 3×10^{-11} radians when rotating at 1 degree/hr. To improve the sensitivity, multiple loops can be added to magnify the Sagnac effect. For a multi-loop configuration, the new effective area is equal to $A_E = N \cdot A$ where N is the number of loops of a FOG. Therefore, a coil with N loops will have a path length difference and phase shift that are both increased by a factor of N resulting with a more sensitive device. This phase difference $\Delta \phi$ can then be measured to obtain the rate of rotation with Equation 1.2 [9].

$$\Delta\phi = \frac{2\pi}{\lambda_0}\Delta L = \frac{8\pi AN}{\lambda_0 c}\Omega \qquad \textbf{Equation 1.2}$$

where λ_0 = wavelength of light in a vacuum
A = area enclosed by the path
N = number of loops
c = speed of light in a vacuum
Ω = rotation rate

In 1913, the French researcher Sagnac first proposed using this concept of phase

shift for measurement and created a demonstration [10]. His simple device consisted of

a light source, a 45° beam splitter, and a ring of mirrors. With this device, he was able to

successfully prove the above concept, which is now commonly known as the Sagnac

Effect. Figure 1.4 illustrates his device called a Sagnac interferometer. The entire device

could be rotated at a velocity Omega and the combined light was shone onto a screen. A

fringe pattern was seen on the screen that shifted directly with rotation Omega. About

sixty years later, in 1976, Vali and Shorthill proposed and implemented the first optical

fiber gyroscope [11]. Since then, the technology has grown to the point where FOGs are

used commercially in many medium-precision applications in preference to more

complex mechanical gyros.
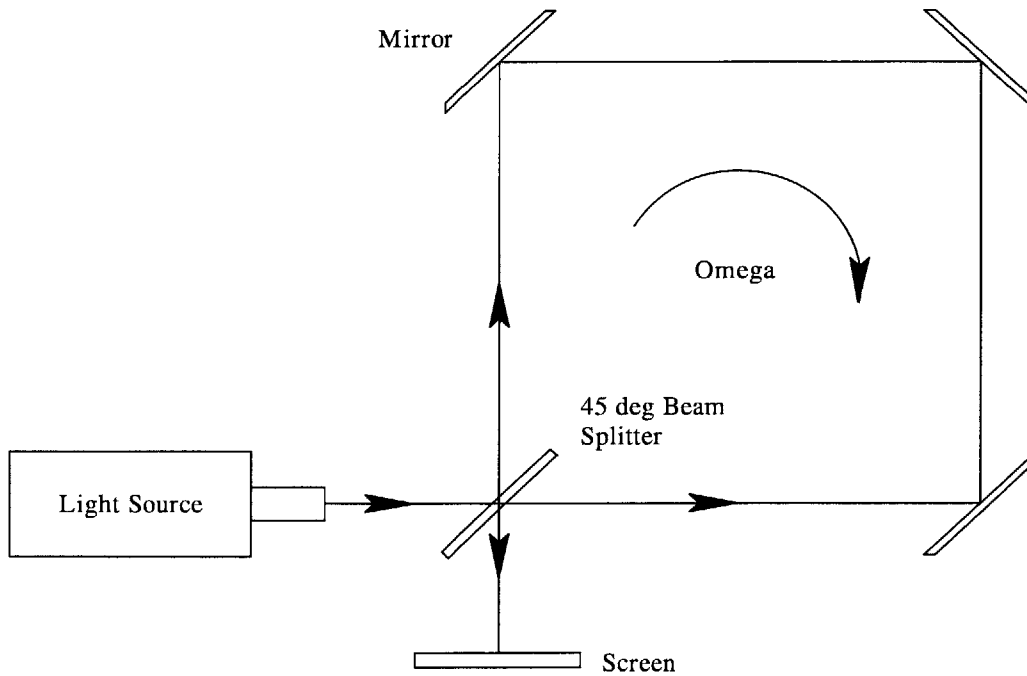
Figure 1.4. The Sagnac interferometer [6]

1.4. Components of a FOG

The major components of a standard fiber optic gyro are shown in Figure 1.5.

These components are the light source, source coupler, integrated optics chip (IOC), coil,

and photodetector. Each of these components will be discussed in more detail in the

following sections.

Light Source

Source Coupler

Photodetector

Modulators

Polarizer

Integrated Optics Chip

Coil
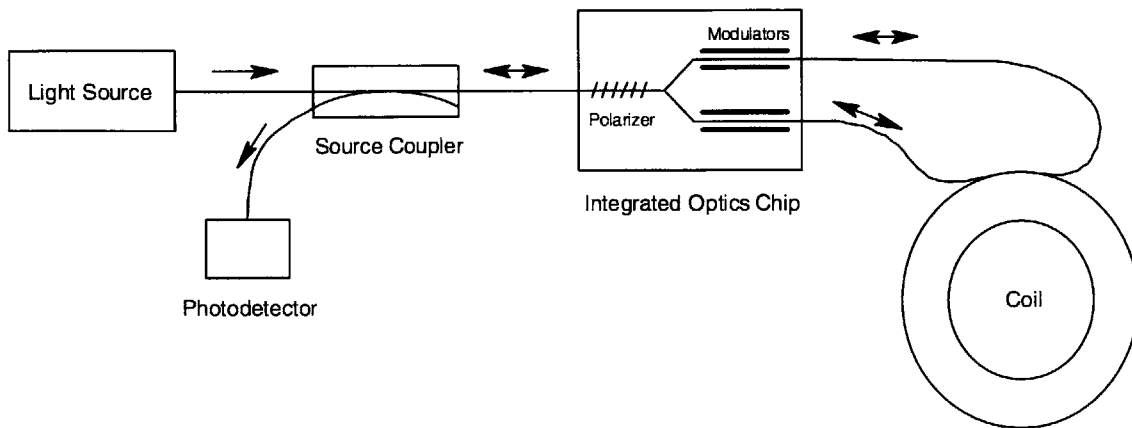
Figure 1.5. Diagram of fiber optic gyroscope [6].

1.4.A. Light Source

The laser is the light source for the gyro. It provides a constant, wavelength

beam of light that drives the Sagnac effect. Laser diodes are commonly used in FOGs as

they have low power requirements and are solid state. For reasons beyond the scope of

this thesis, laser output is often sent to a rare-earth doped fiber that acts to amplify the

beam and spread its spectrum. Together, the diode and doped fiber form the light

source for the gyro.

1.4.B. Source Coupler

The source coupler serves the basic traffic-cop function of routing light to the coil

and back to the photodetector. Light from the source is sent to the coil (with a –3dB split

loss) and light returning from the coil is directed to the photodetector (again with a –3dB

split loss). A coupler consists of two fibers fused together along their sides and reinforced for durability. A fiber lead coming from the laser attaches to the end of one of the fibers and the lead from the coil is attached to the other end of the same fiber. The photodetector lead is attached to the other fiber on the same end of the coupler as the source. Finally, the remaining coupler fiber end is left unconnected.

1.4.C. Integrated Optics Chip (IOC)

In order to create the two light beams for the coil, a beam splitting optical device must be used. This splitter also serves the purpose of recombining the two light beams returning from the coil. While there are various forms of splitters available, a special type called an Integrated Optics Chip (IOC) is commonly used in gyroscopes. Waveguides are formed near the surface of the chip to efficiently direct and apportion the light between the single fiber and the two coil fiber ends. The IOC looks much like a rectangular piece of glass with the fibers attached to the shorter ends of the rectangle. The IOC is different from other beam splitter technologies because of its electro-optical active region that can use electrical input signals to modulate the phase of the light, a necessary feature of being able to produce a useful gyro output. The IOC waveguide also acts as a powerful polarized ion filter, which enhances gyro performance.

1.4.D. Photodetector

In order to monitor the relative phase of the light emerging from the coil, the returning beams are imaged onto a photodetector. Changes in phase (i.e. in interference), cause a change in light intensity on the detector. As photons of light contact a specially designed semiconductor surface, free electrons are created which flow through an electrical circuit on the semiconductor surface. The resulting measurable current is a function of the total light intensity.

1.4.E. Coil

The fiber optic coil has the most bearing on this document since this project's goal was to improve coil performance. Therefore, the many unique features of the coil will be covered in much more detail than the other components. Many of the references cited thoroughly discuss the other FOG components.

1.5. FOG Performance

A common measure of a gyro's performance is its drift rate. This corresponds to rotation sensing error over time (degrees/hour). The best gyros have better than .001 deg/hr of drift, termed strategic grade, the next best have .01 deg/hr, termed navigation grade, and the crudest coils have 1 deg/hr, termed tactical grade. With current technology, tactical grade coils are relatively easy to wind. Navigation grade coils are commonly produced but at high costs and at low production rates. Strategic grade coils can be wound, but they require a great deal of care and are highly labor intensive. To be

27

used for navigation applications, the gyros must be of navigation grade or better to avoid excess error in the sensor readings [6].

Three main coil parameters can affect a high performance FOG: first, the Shupe effect due to a moving temperature gradient [12], second, the Faraday magnetic effect scatter, and finally, bias drift related to polarization scatter. Each of these effects will be discussed in more detail.

1.5.A. Shupe Effect

The Sagnac effect assumes that a coil's rotation is the sole cause for a measurable phase shift; however, other non-reciprocal factors can create shifts that cannot be distinguished from Sagnac effects. For example, D. M. Shupe showed that a moving temperature gradient pattern in a coil could generate a phase shift between the counter-rotating beams [12]. This phenomenon, known as the Shupe Effect, occurs because the light propagation velocity (the index of refraction) is a function of temperature. Therefore, if temperature is changing with time, the velocity of light in the fiber will be different at the moment the first beam passes then an instant later when the opposite beam passes. The result is a gyro that senses a phase shift not caused by experiencing a rotation. Figure 1.6 illustrates this point.

Different approaches can minimize the Shupe Effect. One method relies on insulating the coil from thermal effects; however, this type of insulation is bulky. Unfortunately, most gyro applications require a compact and small package. A second method suggested by Shupe involves altering the coil winding geometry. The approach is to create winding patterns that achieve maximum symmetry within the coil [12]. By

28

doing this, light traveling in opposite directions will see the same variations at the same

time as it passes through the fiber. Hence, any change experienced by one of the beams

should be virtually identical to that of the other, and when recombined, the two

propagating light beams should only reflect phase shifts due to rotation [13]. Figure 1.7

provides a clarification of this concept.
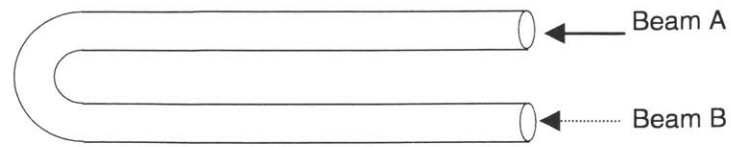
Beam A

Beam B

At some time t = 0, both
beams are launched

Temp. gradient at position x
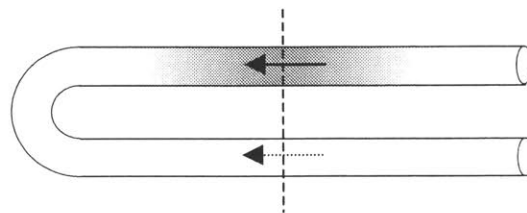
At t = t_1, only Beam A experiences a local
temp. gradient and hence speed
of light has changed locally.

Temp. gradient disappears
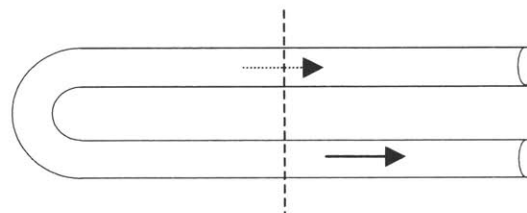
At t = t_2, the counter-propagating Beam B does not
experience the same temp. gradient as Beam A;
therefore, the two beams will emerge with a phase shift.

Figure 1.6. Overview of performance affects from a
temperature gradient changing with respect to time.

Beam A

Beam B
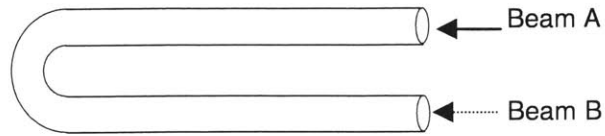
At some time t = 0, both
beams are launched

With anti-Shupe winding

Temp. gradient at position **x**
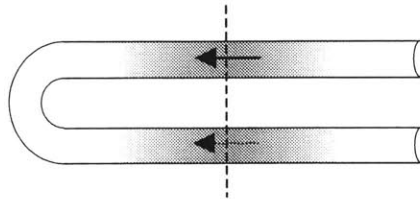
At t = t_1, both beams experience a temperature
gradient and hence the speed of light has
changed locally in two places by same amount.
Positions of fiber carrying counter-propagating
beams are placed in close proximity to assure
they have nearly identical temperatures and
therefore minimal reciprocity.

Temp. gradient disappears
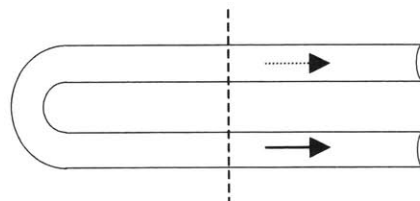
At t = t_2, since both beams experienced the
temp. gradient at the same time, both emerge
in phase.

Figure 1.7. By using an anti-Shupe winding scheme, errors
from temperature gradients are minimized.

31

To wind the fiber with such symmetry, the coil must actually be wound in a special way. More specifically, winding must start with the midpoint of the fiber and proceed outwards in alternate-direction layers. Half the fiber will be wound clockwise around the coil and the other half counterclockwise. This will lead to a coil that has the fiber ends exiting the coil on the outside diameter and in opposite directions, as shown in Figure 1.8. To actually wind a coil this way, a length of fiber must first be wound half onto one supply spool and half on another, with the midpoint of the fiber between the supply spools [14]. During winding, the supply spools will pay out fiber onto the product spool, which holds the coil. At any one time during a wind, one supply spool will be actively paying out fiber while the other is locked in place, rotating as the product spool rotates. An example sequence of winding is shown in Figure 1.9. Note the two supply spools containing half the fiber and the inactive and active positions for each spool.
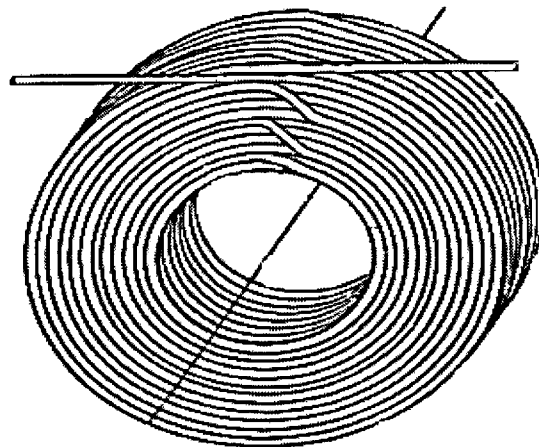
Figure 1.8. A fiber optic gyroscope coil [14].

32

Supply spool with
half the fiber to be
wound

Midpoint of fiber

Supply spool with
half the fiber to be
wound

Active supply
spool pays out
fiber

Product spool
containing FOG
coil takes up fiber

Inactive supply spool turns
with product spool, not
paying out fiber
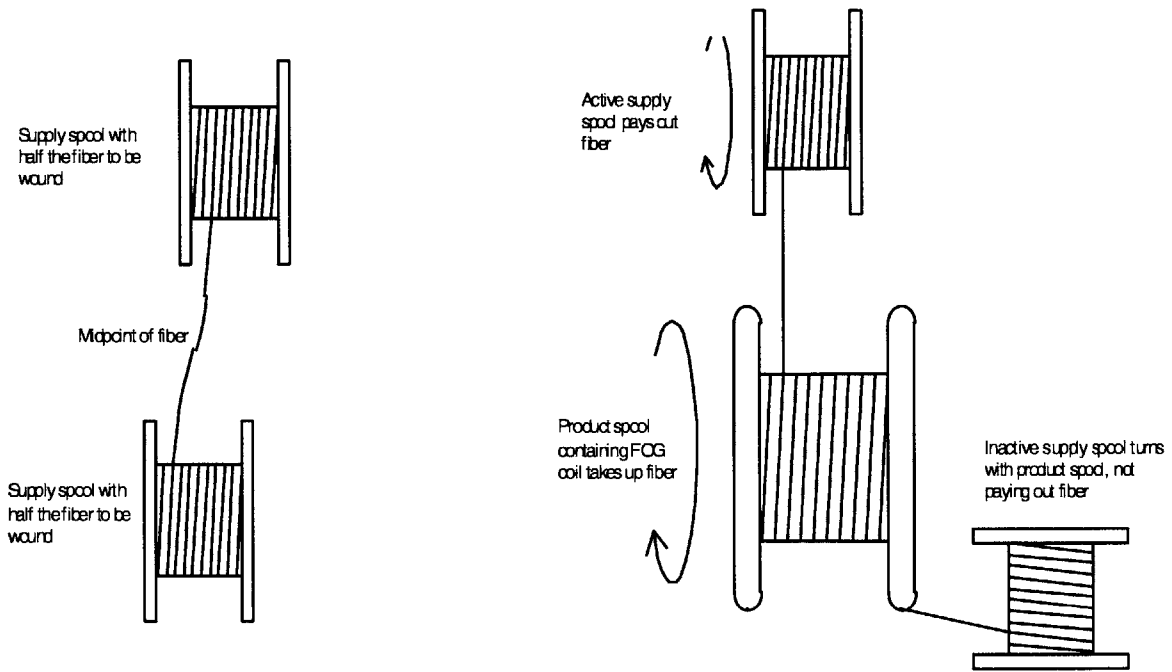
**1. Fiber is divided between the
two supply spools.**

**2. One supply spool pays out fiber while
the other remains inactive.**

Product spool takes up
fiber, now rotating in the
opposite direction
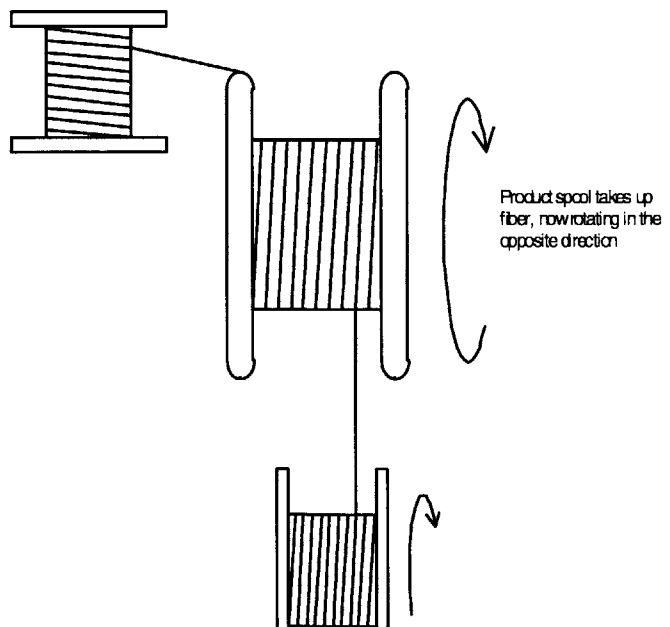
**4. The two supply spools alternate
paying out fiber until the coil is
completed.**

Figure 1.9. Winding sequence [6]

33

Keeping in mind that coils are wound in this inside-out manner, there are various patterns of fiber placement that can result in coil symmetry, some exhibiting better results than others. The most often used pattern is termed a "quadrupole wind." Figure 1.10 depicts a cross-section of a coil wound with this pattern. The white circles indicate fibers wound in one direction and the black indicate those fibers wound in the other. By examination, it can be seen that corresponding turns of the black and white fiber are in very close proximity within the fiber pack. Also note that underlying layers of fiber form grooves which subsequent layers use to guide fiber leading to a tighter pack. The exception being the base layer that is sometimes wound on grooved mandrel (not shown).
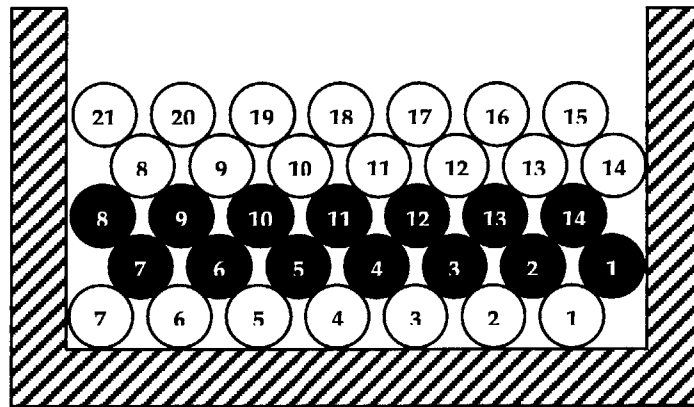
Figure 1.10. Cross-section of a coil wound in a quadrupole pattern.

1.5.B. Magnetic Field Sensitivity: Faraday Effect

Another issue with a high performance gyro is sensitivity to magnetic fields, the Faraday effect. This effect depends on the relationship between voltage and a time-varying magnetic field [15]. Since light can be described as an electromagnetic wave, the Faraday effect has implications for a fiber optic gyroscope.

Suppose a magnetic field is imposed on guided light such as in a strand of optical fiber that is transmitting polarized light. The Faraday effect will cause the light to emerge with its polarization axis slightly rotated (see Figure 1.11). In the case of polarization maintaining fiber (PM fiber) where the propagation velocity is different in the two principal axes, polarized light from one axis will enter the other axis. This results in the counter rotating light beams changing phase with respect to each other, creating an apparent inertial rotation. Since this error can be calculated, a measured value can be adjusted for this error as long as the fiber's orientation in the magnetic field and the field strength remain constant.

If the polarization field within the fiber rotates by an unknown amount due to an inconstant magnetic field, the resulting Faraday drift can not be calculated. Specifically, Hotate and Tabe show that drift is worst within a FOG when the fiber's longitudinal twist has a period equal to one turn of the sensing coil [16]. The future work section of this thesis will discuss methods for reducing this effect.

Magnetic field

Light enters with specific polarization

Optical

Light exits with different polarization
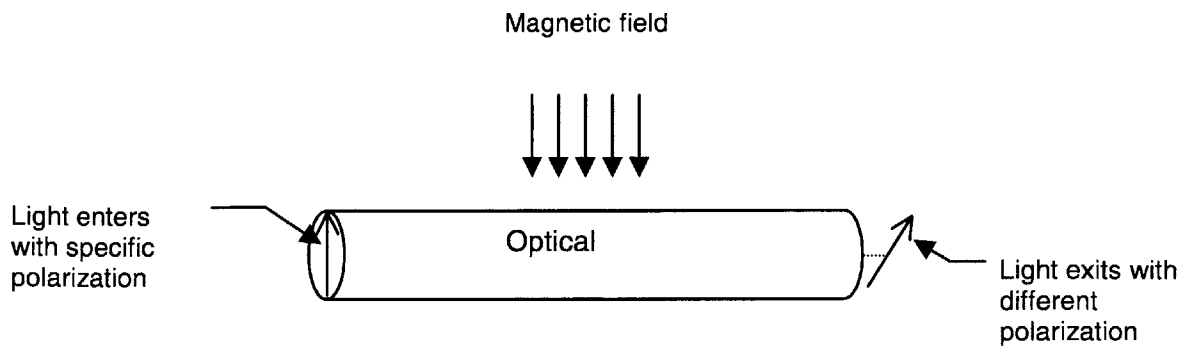
Figure 1.11. A polarized light beam experiences net rotation when exposed to a magnetic field.

1.5.C. Minimizing polarization crosstalk

High performance FOGs have normally been built using low crosstalk PM fiber. The two counter-rotating optical signals are launched into the same fiber axis, where they travel at virtually identical velocities. PM fiber keeps light from rotating into the orthogonal polarization by taking advantage of the fact that in glass the index of refraction is a function of stress. Imposing a large principal stress along one direction creates two distinct indices (see Figure 1.12), and allows two polarized beams to remain isolated.

If this principal stress is altered or rotated in any way, the light polarization will follow, creating polarization crosstalk or leakage of light into the orthogonal polarization, which could incorrectly be perceived as a rotation rate. To counter this effect, stress disruptions should be minimized.

36
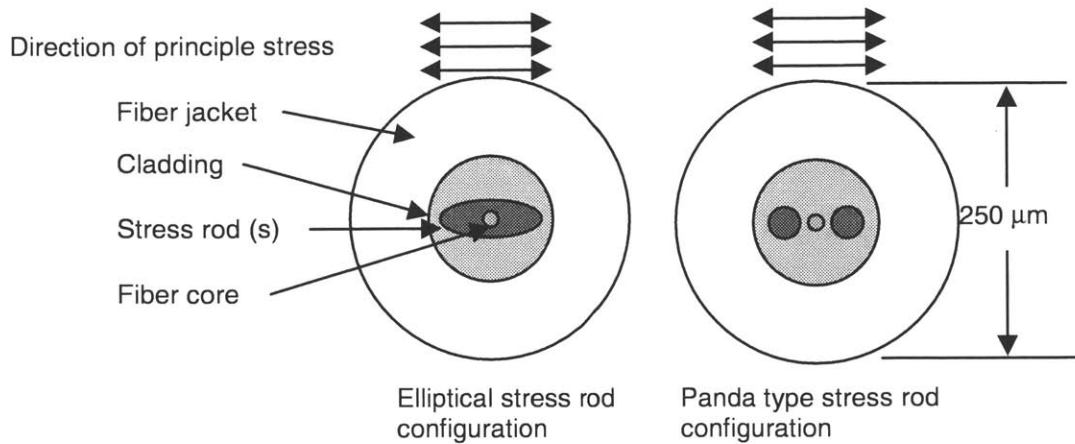
Figure 1.12. These polarization maintaining fiber cross-sections show two common stress rod configurations.

Regardless of the specific coil winding pattern, localized stress concentrations on the coil fiber can adversely affect coil performance. Certain discontinuities in stress, known as microbending, arise from fiber crossover regions. Figure 1.10 depicts a typical quadrupole wind; white circles denote one end of the fiber and black circles denote the other end. As a turn of fiber makes its transition from position 1 (black) to position 2 (black), it must cross over a fiber cross-section labeled 1 (white). This results with point contact causing a substantial disturbance to the PM fiber's internal stress field.

Two actions can minimize microbending and polarization crosstalk: lower winding tension and fewer crossovers. A lower winding tension decreases the point contact stress. Issues with reducing the winding tension will be discussed in detail in Chapter 2. By changing the winding geometry, one can minimize the number of crossovers, which in turn decreases the number of polarization crosstalk locations.

The most intuitive method to wind a coil is in a spiral or helix pattern. The fiber is allowed to traverse across the pack naturally as it is wound onto the coil. If the fiber is

wound at the same helix angle as the previous layer, it follows grooves formed by that

layer. However, if it is wound at the reverse helix angle as shown in Figure 1.13, the

fiber has no set groove to follow. Instead, its track will meander in and out of the groove

in the lower level. One can see that this phenomenon can cause inconsistencies in each

layer, which can only get worse on subsequent layers. An example of a cross-section of

a coil wound in this way is shown in Figure 1.14.
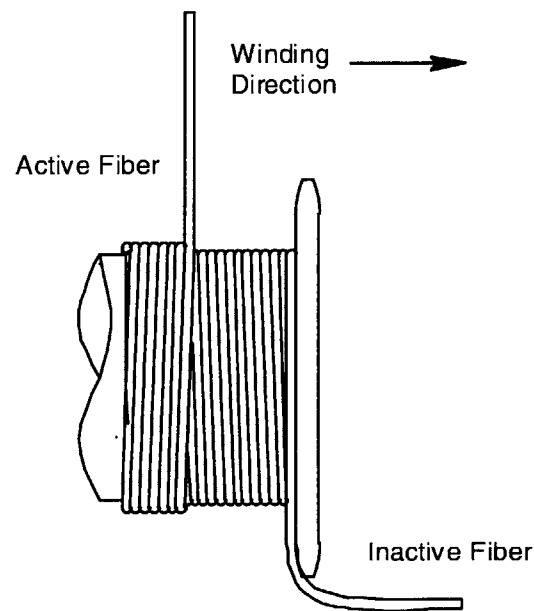
Figure 1.13. Helical winding technique leads to inconsistencies in each layer. When the traversing direction is reversed, the current layer has no set track to follow. Thus, the fiber will meander in and out of the underlying grooves [6].
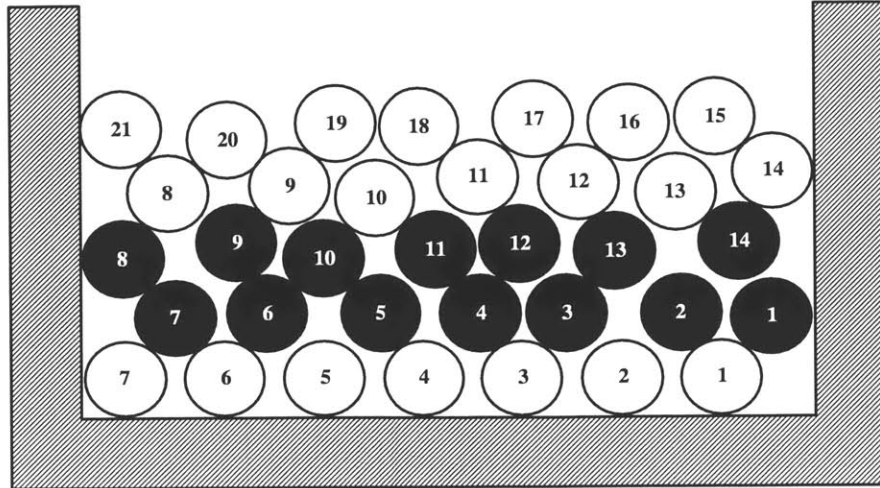
Figure 1.14. Helical wind cross section shows that since a layer can not follow the grooves formed by the underlying layer, it becomes inconsistent.

One alternative winding method is called an orthocyclic wind. This winding method was first developed by Phillips Industries in 1962 and is commonly used today [17]. With this method, rather than winding in a helix, fibers are wound in concentric hoops and cross over to adjacent grooves formed by the under-lying layer in well-defined zones. See Figure 1.15 for an illustration of this type of wind. The zone where the fibers cross grooves is commonly termed the "jog zone" and is the only location in the coil where fibers deviate from a concentric orientation.

Many advantages are gleaned from orthocyclic winding. Local stresses due to crossing over are limited to one small area of the coil. Also, the majority of the coil's circumference is wound with an even, closely packed profile much like that shown in Figure 1.10. Any inconsistencies should only occur in the tight jog zone. Finally, the

close pack inherent to the orthocyclic wind has been shown to improve the thermal

variation and vibration resistance of the coil [6].
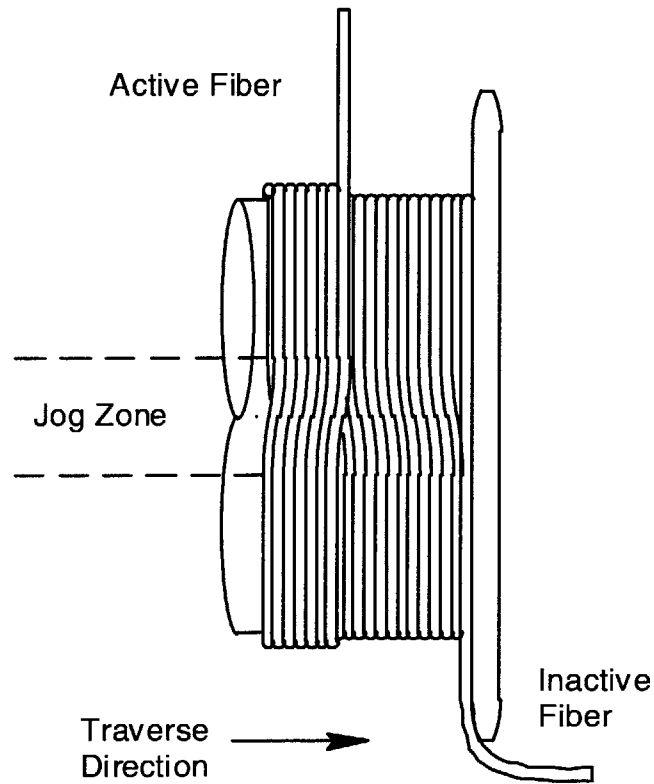
Figure 1.15. Orthocyclic winding forces all cross-overs to occur in a localized region called a jog zone. As fiber traverses in either direction, it will lay in concentric grooves formed by the underlying layer [6].

1.6. Improving Coil Performance

Of the three mechanisms that affect high performance FOGs, this thesis focuses on minimizing polarization crosstalk. This can be addressed primarily by reducing the winding tension. Several complications arise from low tensions such as the increased importance of higher order effects like elastic twist in fiber. Chapter 2 discusses alterations to the coil winder and processing of optical fiber to reduce these higher order effects. Chapter 3 provides details on the embodiment of a suggested algorithm for untwisting optical fiber into a fully automated fiber optic untwisting machine (AFOUM). Results from several untwisting trials are presented and analyzed in Chapter 4. Finally, Chapter 5 suggests possible avenues for future work that emphasizes optical untwisting as an avenue for mitigating magnetic sensitivity.

CHAPTER 2   REDUCTION OF TENSION

As mentioned in Chapter 1, one mechanism for reducing polarization crosstalk is

to lower the winding tension. Several issues arise during a low tension wind, including

some significant errors caused by elastic twist in the fiber. This chapter will discuss in

detail the sources of each error component and solutions to minimize polarization

losses.

2.1.   *Consequences of reducing winding tension*

A set of experiments were conducted that involved winding coils at low tension.

As mentioned in Chapter 1, the motivation for winding at low tensions is to improve the

polarity maintaining ability of PM fiber. This section will discuss the effects of lower

winding tensions.

2.1.A. Larger jog-zone angle

Coil winding often requires a fiber strand to be precisely positioned into a small,

lateral arc (radius ≤ 1 inch). As shown by Equation 2.1, as the point load to a

cantilevered beam is decreased the radius of curvature increases (please refer to the

Appendix A for a more detailed derivation). This means that as the tension is decreased,

the more difficult it becomes to place a fiber strand into a tight radius. This issue arises

in winding through the jog-zone.

$$\frac{1}{\rho} = \frac{d\theta}{ds} = \frac{P(L-x)}{EI}$$

Equation 2.1

Ideally, one would like a very small jog-zone. This increases the probability that fiber positioning will be deterministic. However, as tension decreases, the designed jog-zone angle must increase. An attempt to hold too small a jog-zone angle with a lower tension usually results in an uncontrollable jog-zone growth. Manual intervention is usually needed to correct this spreading jog-zone.

2.1.B. Gap errors from twist

Another phenomenon arises when winding tension is lowered. While winding onto a grooveless mandrel, the MIT Manufacturing Institute (MIT/MI) observed gap errors (excessive space between adjacent fiber turns) that progressively grew as the mandrel rotated (see Figure 2.1). It appeared that, the fiber was rolling up a lower layer fiber to a position higher than surrounding fiber turns. This raised suspicion that the fiber had some type of torsional twist. The only way to correct this error was to unwind back to the gap, remove the supply spool, untwist the fiber by hand, replace the spool, and continue winding.
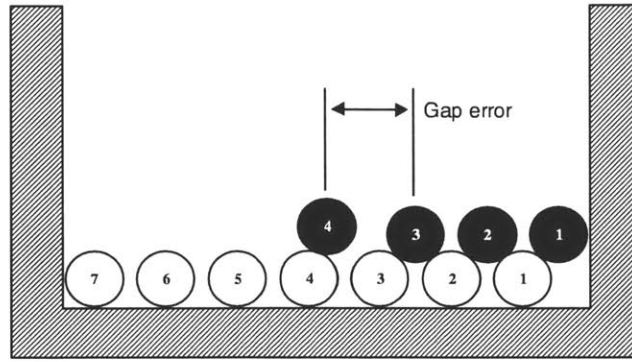
Figure 2.1. Illustration of a gap error

A simple experiment was concocted to test the theory that twist was responsible for the progressively increasing gap error. First a sample strand of fiber was measured to approximately 3 feet. This sample was wound at 6 grams of tension onto a 2.8 inch diameter mandrel with no grooves (this is approximately 4 turns). This served as a control. The wind was analyzed and determined to be satisfactory. Next, the fiber was unwound and taken off the supply spool. One full turn of twist was manually applied, the fiber was restored onto the supply spool, and rewound onto the mandrel with all machine parameters at their previous settings. Within four turns, a gap appeared and began to progressively increase in width. This same experiment was repeated with two, three, and four turns of twist; each trial resulted in gap formation, with width proportional to the total manually-applied twist.

Another series of experiments involved varying the tension between four and ten grams with only one turn of twist. At four grams, the fiber behaved very similarly to the previous trial; however, as the tension was raised to ten grams, gap formation was markedly reduced. From this experiment, it was concluded that the fiber's tendency to roll out of its intended track was reduced by higher tensions. The lateral component of the tension was greater than the frictional force between the fiber jacket and mandrel; therefore, the fiber would assume its intended position (see Figure 2.2).
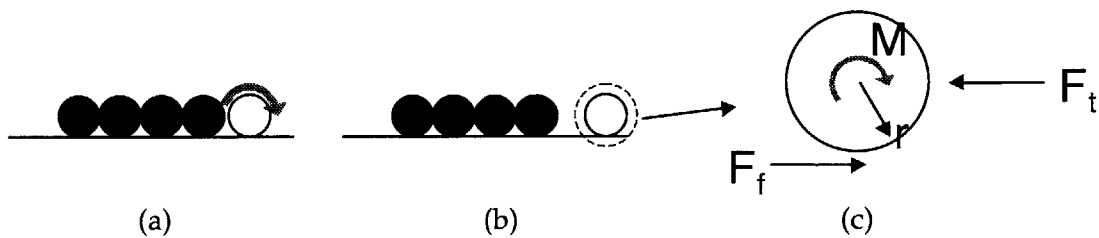
Figure 2.2. Torsion in fiber (a) creates a moment, M, that creates a tendency for the current turn to roll away (b). A higher winding tension, F_t, can overcome the frictional force, $F_f = r M$ (c).

2.2. Sources of twist

Since experiments had shown that twist could affect fiber placement, the next step involved determining sources of twist in fiber. A thorough investigation developed three theories.

2.2.A. Lag-angles

The first theory examines the winding process itself and theorizes that lag angles normally utilized to pull the fiber closer to the fiber pack were actually causing a differential in velocity that caused twist. As shown in Figure 2.3, as a fiber with a lag angle approaches an adjacent fiber, it's outer jacket sees an instantaneous velocity of zero while its center continues to move down. This results with twist.
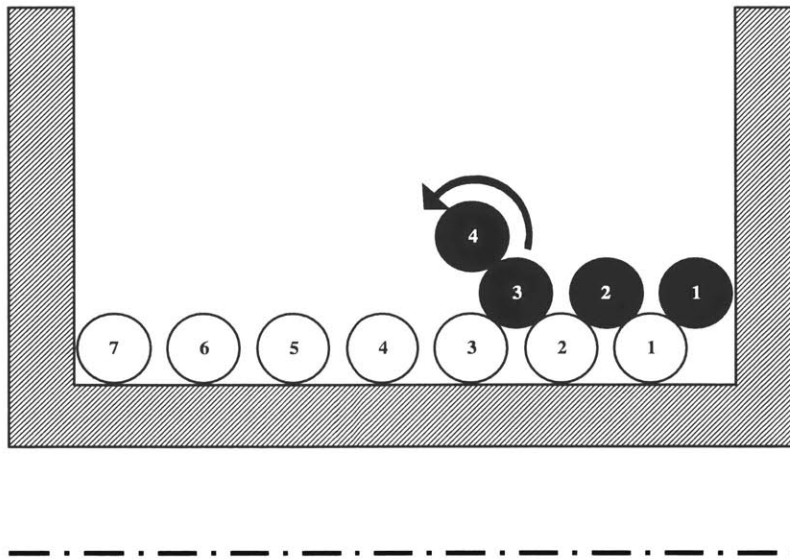
Figure 2.3. Using a large lag angle forces the current turn of fiber to rub against a previously placed fiber. This induces twist in the current turn of fiber.

To correct this problem, one could simply eliminate the lag angle; however, as observed during previous winding experiments, a zero lag angle setting as a winding

parameter would generally cause the fiber to roll into another equilibrium position. The assumption is that the coil winder's positional accuracy was sufficient enough to guarantee a near-zero lag angle. Thus, there had to be another explanation for the source of twist.

2.2.B. Curvature of fiber

A second theory involved tracing the fiber path on the coil winder. Inspection of the winding machine showed that the fiber's curvature was being reversed between the supply spool and the mandrel. This effect would intensify if fiber was left on the supply spool for more than two days. Over this period, the fiber would develop a curvature memory to that specific supply spool. Winding at this state under low tension would allow fiber to try to assume its memory curvature by twisting over itself (see Figure 2.4).
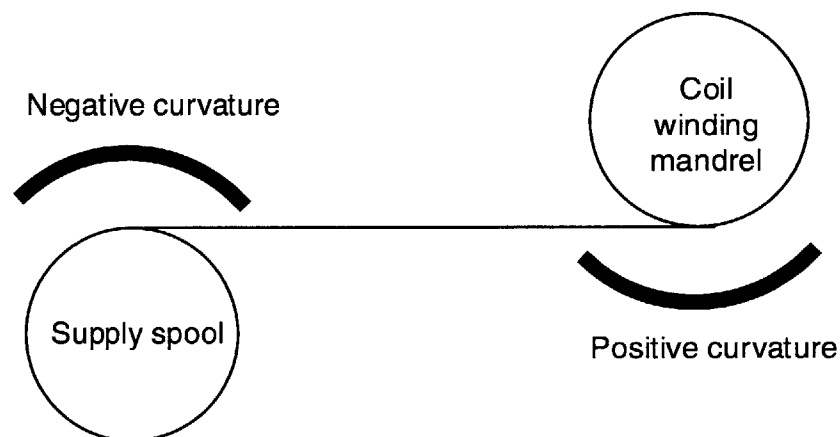
Figure 2.4. Fiber on the coil winder's supply spool had a negative curvature, but the gyro was wound with positive curvature. This would induce twist since the fiber has a tendency to roll back to negative curvature.

A solution to this problem involved inverting the direction fiber was paid-out from the supply spool. Since the supply spool is driven with a small, brushed DC servo motor, the motor power leads were simply reversed (see Figure 2.5). This solution would alleviate the problem for fiber left on the supply spool for long periods; however, previous experiments had shown that even fresh fiber (less than 1 day on a supply spool) experienced twist related gapping errors. Therefore, yet another theory was needed to explain the source of twist.
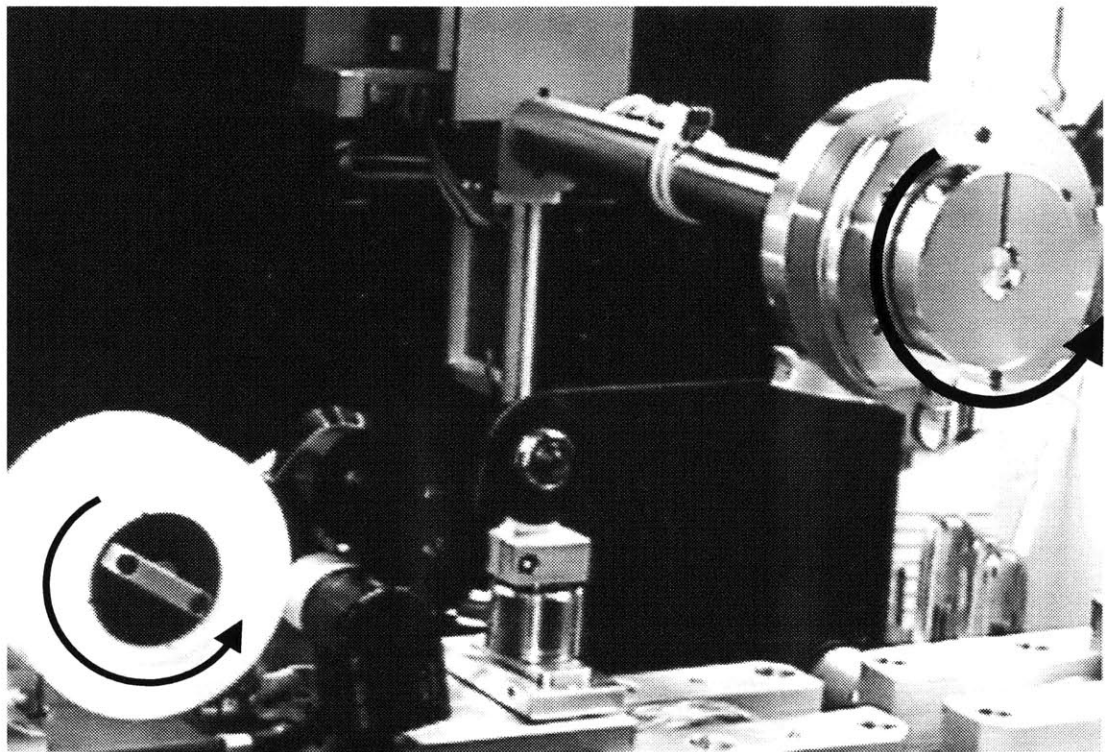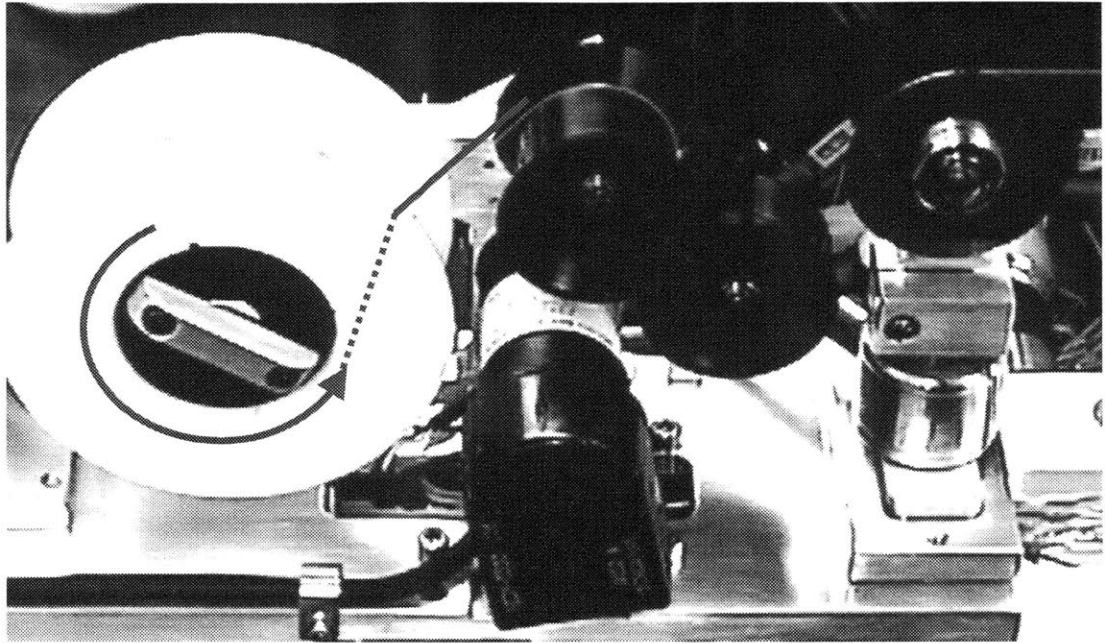
Figure 2.5. (top) The DC motor's polarity was inverted so fiber could payout from the underside of the supply spool. (bottom) Curvature on supply spool matches curvature on product spool.

2.2.C. Fiber manufacturing and handling

The last investigation focused on the history of fiber handling. The culprit had to be a process occurring before a supply spool was mounted onto the coil winder. After careful examination of the transfer winding process, the MIT/MI determined that fiber twist was most likely built into the fiber on the supply spool as received from the manufacturer.

Figure 2.6 shows a diagram of a typical fiber draw tower. The manufacturing process begins with a pre-form that is pulled through an inductive furnace. Draw rate and furnace temperature are used to control the diameter of the fiber cladding. Protective jacketing is applied in the same line, usually as two layers of polymeric coatings. A capstan wheel and a take up spool provide the tension needed to draw the pre-form through the inductive furnace. A closer look at this capstan reveals a not so obvious source of twist.

Since the capstan roller has a flat across its diameter, a fiber has a tendency to walk back and forth essentially hunting for an equilibrium position as it moves across the capstan's surface (see Figure 2.7). In order to move from one position to another, the fiber must roll if the frictional force between it and the capstan's surface is high. This rolling twists the fiber. Since a finite distance separates the flanges of the capstan, the magnitude of twist is bounded in both directions. Thus, if one integrates twist over the full length of the fiber, the total accumulated twist would be bounded and centered about zero.
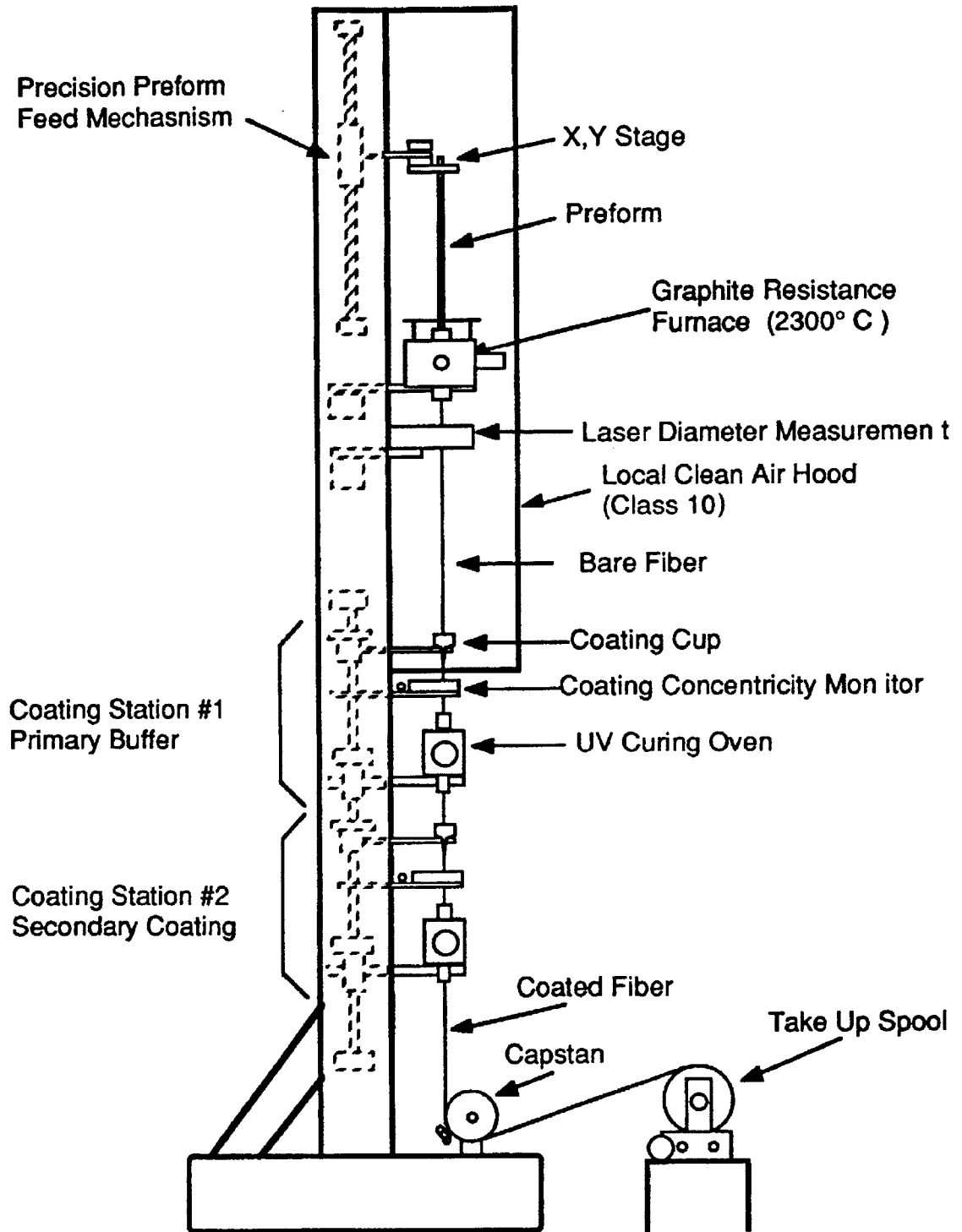
Figure 2.6. Optical fiber is manufactured using a draw tower (typically 10m tall). An unconfirmed source of twist is the capstan roller (picture provided by an anonymous fiber manufacturer).

The labels in the figure read:

Precision Preform Feed Mechasnism

X,Y Stage

Preform

Graphite Resistance Furnace (2300° C)

Laser Diameter Measuremen t

Local Clean Air Hood (Class 10)

Bare Fiber

Coating Cup

Coating Concentricity Mon itor

Coating Station #1 Primary Buffer

UV Curing Oven

Coating Station #2 Secondary Coating

Coated Fiber

Capstan

Take Up Spool

Two independent fiber manufacturers have observed this phenomenon. Both have observed the fiber walking from flange to flange on the capstan. Given the real possibility of twist built into fiber, the MIT/MI decided to focus on means for undoing that twist.
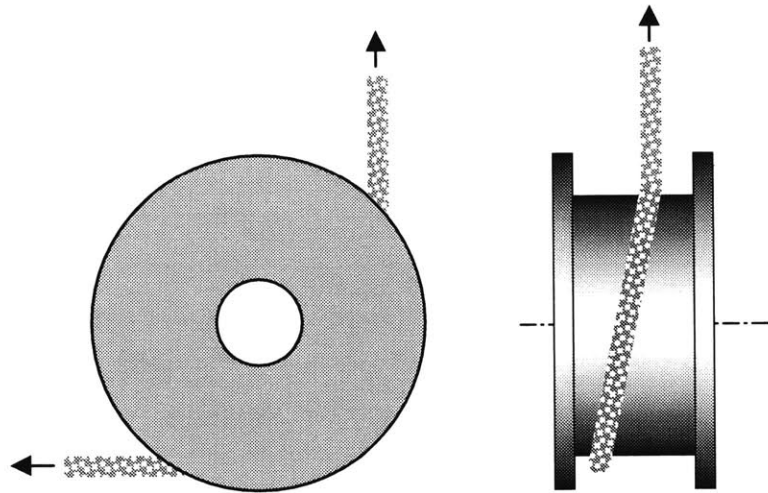
Figure 2.7. One hypothesis for twisted fiber is wander on the flat of the capstan roller. This flat allows the fiber to roll from flange to flange inducing a periodic twist.

2.2.D. Approach to eliminating twist

An obvious starting point would be working with fiber manufacturers. Two main factors made this option not feasible. First, fiber manufacturers would have to provide proprietary process information. Although special agreements exist for similar cases, this avenue was not workable. The second factor is probably the most important consideration. Eliminating the small amounts of twist would benefit only a very small fraction of fiber customers who want to wind low-tension, precision coils. Therefore, a

fiber manufacturer would derive little market benefit from sharing the process

information. This further encouraged the MIT/MI to investigate twist removal

techniques after the fiber has been delivered.

CHAPTER 3 DESIGN OF AN UNTWISTING MACHINE

The first step in eliminating twist from fiber was to apply the fundamentals of

mechanics and to model twisted fiber. This model led to the development of a simple,

open-loop untwisting process. The next step involved decomposing the proposed

untwisting process into a hierarchy of functional needs and design parameters. These

three steps created the Automated Fiber Optic Untwisting Machine (AFOUM).

3.1.   Static and Dynamic Torsional Analysis

Creating a static and dynamic model of the fiber proved to be an invaluable

process. The static model helped establish the necessary sensitivity and precision for an

untwisting process, while the dynamic model formed the basis for the untwisting

principal of operation.

3.1.A. Static twist characterization

A simple static torsional analysis allowed better understanding of the mechanics

behind twist. A basic torsion relation in Equation 3.1 was used to calculate the

magnitude of torque for a given torsional strain. This showed that 0.007oz-in (0.005 N-

mm) of torque was needed to twist a 1 meter length of fiber 90 degrees (see Table 3.1).

Therefore, achieving a 1 deg. rotational precision would require 0.00008 oz-in (0.0006 N-

mm) of torque resolution.

$$\phi = \frac{TL}{GI_p}$$

Equation 3.1 [18]

where ϕ = total torsional strain angle

T = applied torque

L = length

G = shear modulus

I_p = polar moment of inertia

Table 3.1. Static torsional analysis

	E	v	G	diameter	diameter	Ip	G*Ip
Fiber Data							
	psi		psi	μm	in	in^4	
Cladding	1.05E+07	0.17	4487179	125	0.004921	5.76E-11	2.58E-04
Inner Jacket	400	0.495	133.7793	187.5	0.007382	2.34E-10	3.13E-08
Outer Jacket	105125	0.46	36001.71	250	0.009843	6.3E-10	2.27E-05
Static Twist Simulation							
L	1	meter					
	Torque	Torque	Phi	Phi			
	(in-lbf)	(oz-in)	rad	deg			
	0.000442	0.007065	1.570796	90			

The next logical step was to craft an experiment to test the feasibility of observing

this ultra-low torque. While brainstorming possible experimental configurations, the

MIT/MI determined that measuring this ultra-low torque directly was not feasible given

existing equipment. A simpler approach was needed. A hypothesis suggested that

characterizing a dynamic response could reveal the necessary information in a slightly

different form.

3.1.B. Dynamic twist characterization

The MIT/MI created an experimental setup to determine a dynamic response. This setup was composed of a length of fiber attached to a supply spool (see Figure 3.1). This geometry was oriented in a vertical fashion and allowed to freely rotate. Several observations were made. First, an ultra-low torque was indeed observable as the rotary oscillation of a second order system. Second, the lack of sufficient damping extended the settling time to an impractical duration. This was confirmed using a second order model created in MatLab (refer to Appendix B for a derivation). Equation 3.2 shows the general form of a damped, second order system. Figure 3.2 shows the behavior of a typical second order system; however, the settling time of greater than 100 seconds for 1 meter segment was considered to be too long for a practical untwisting device. Thus, the concept of merely allowing an oscillating mass to settle to a zero torsional strain was abandoned.
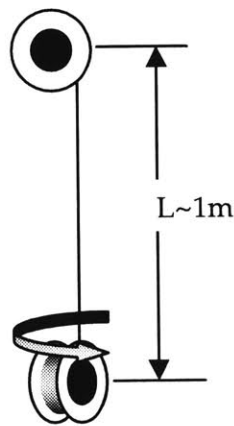
Figure 3.1. Dynamic experimental configuration consisted of two spools. The upper one was kept fixed while the lower spool could freely rotate.
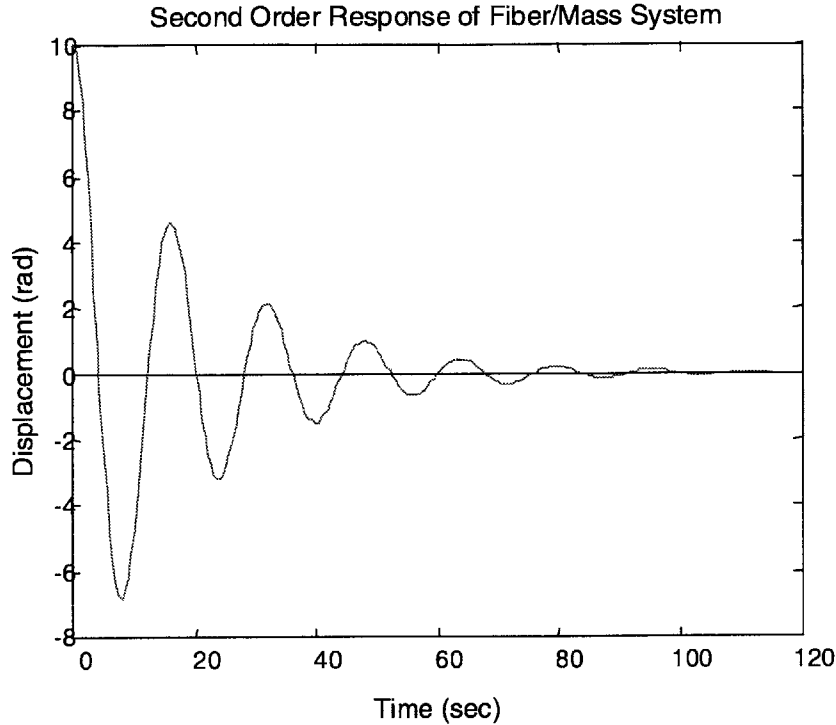
Figure 3.2. Simulation of a fiber/mass system with an initial angular displacement shows a settling time that was too long ($\omega_n = 0.385$, $\zeta = 0.125$).

$$\tau = J\ddot{\theta} + 2\zeta\omega_n\dot{\theta} + k\theta$$

where $\tau = applied\ torque$

$J = moment\ of\ inertia$

$\zeta = damping\ factor$

$\omega_n = natural\ frequency$

$k = torsional\ stiffness$

$\theta = angular\ displacement$

Equation 3.2

The next model examined the effect of different initial angles of twist, ϕ_0. As

shown in Figure 3.3, oscillations beginning with different initial conditions all reach the

equilibrium point at the same time. In addition, solution of the equation for damped

58

natural frequency (see Equation 3.3) yields a constant, so the time to reach each zero-strain crossing is unaffected by initial conditions. This observation led the MIT/MI to formulate a design conception.

Second Order Response of Fiber/Mass System
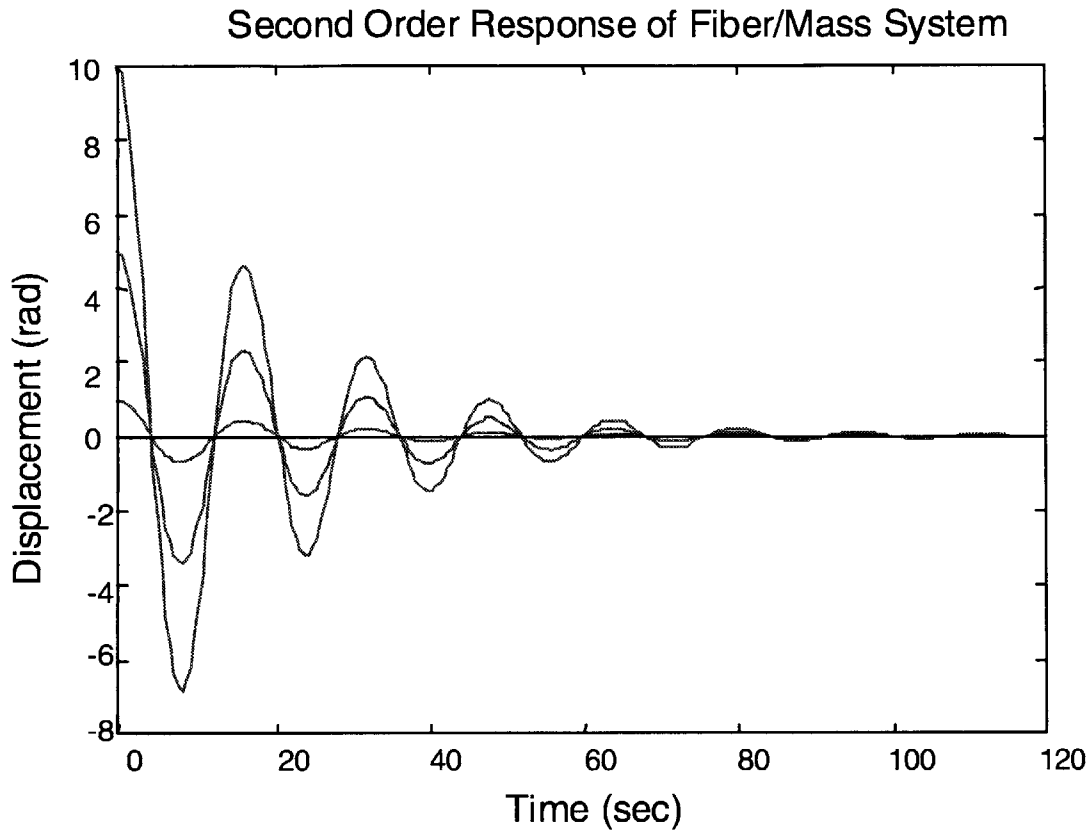
Figure 3.3. Dynamic response of a second order system with different initial conditions shows that zero-strain crossings occur at the same time.

$$\omega_d = \omega_n \sqrt{1-\zeta^2}$$

where ω_d = damped natural frequency $\qquad$ **Equation 3.3**

$\qquad \omega_n$ = natural frequency

$\qquad \zeta$ = damping constant

3.2. Untwisting process conception

A possible untwisting process could utilize this equilibrium time constant to arrest an oscillating mass at the equilibrium point in a simple, open loop procedure. Therefore, this process would untwist discrete fiber sections, each having the exact same length. After untwisting, a take-up spool would wind up the processed fiber, and another spool would dispense another discrete section of fiber. This process would repeat until the entire length has been untwisted.

3.3. Functional Requirements and Design Parameters

The design of the Automated Fiber Optic Untwisting Machine (AFOUM) began with a detailed characterization of functional requirements and design parameters. This process began with high level functional requirements and design parameters that were later broken down into sub-levels. This process of decomposing each level continued until the design parameters reached physical components.

The highest level of functional requirements (FR's) are listed in Table 3.2. These five basic FR's form the foundation of the AFOUM design goals. To achieve these goals, the associated design parameters must be decomposed into sub-levels. At this point, one can observe that the five design parameters contain three unique subsystems: a fiber payout unit, an untwisting subsystem, and a take-up system.

Table 3.2. Highest design level

Functional Requirement		Design Parameter
A.	Payout fiber	Fiber payout subsystem
B.	Untwist fiber	Untwisting subsystem
C.	Collect untwisted fiber	Take-up subsystem
D.	Precision transfer wind	Transfer winder
E.	Do not damage fiber	Safety features

Next, the MIT/MI decided to freeze the relative arrangement and orientation of each subsystem. One possible design layout involved placing the take-up subsystem on the untwisting subsystem. The major disadvantage to this orientation was a substantial increase in the mass moment of inertia and the lengthening of the zero-crossing period. To minimize this effect, the chosen design layout decouples the take-up subsystem from the untwisting mechanism. However, this design layout couples the fiber payout system with the untwisting mechanism. The inertia associated with the fiber payout system was estimated to be significantly lower than the take-up system. Thus, Figures 3.4-3.6 show the proposed design layout and untwisting process.
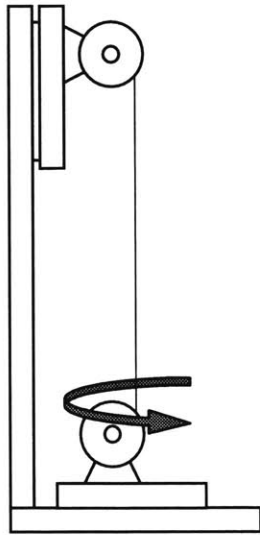
Figure 3.4. Fiber untwists and machine locks lower spool's position
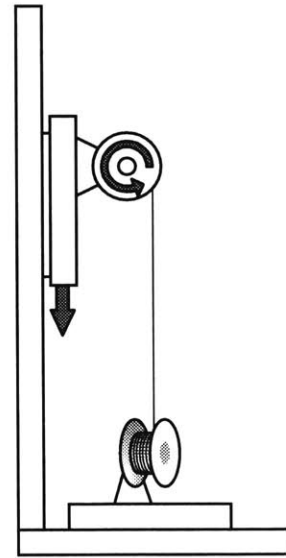
Figure 3.5. Upper spool winds up untwisted fiber
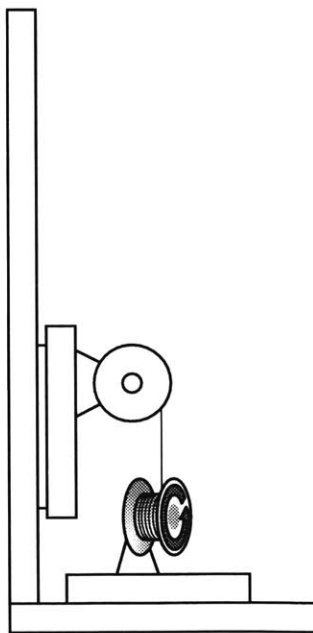
Figure 3.6. Lower spool dispenses fiber while upper spool moves back to original position

3.3.A. Fiber payout subsystem

With an overall layout being frozen, the fiber payout unit can now be broken

down into three sub FR's (see Table 3.3). For the given process, the fiber payout unit has

to maintain tension while it dispenses fiber. The associated design parameter had to be

a passive tensioning mechanism since an active tensioning mechanism would add

significant inertia and complexity. The main implementation issue with an active

mechanism was powering an actuator on a rotating platform. Although this

arrangement is quite feasible with readily available slip-rings, this design was deemed

too complex and unnecessarily expensive. The second FR's design parameter was a

quick disconnect mechanism for attaching and releasing a spool of twisted fiber to the

untwisting platform. This FR came directly from interviewing the AFOUM's future

operator. Finally, since the fiber payout unit rests on the untwisting subsystem, material

selection becomes an important design parameter. Thus, the next step in this design

process decomposes the first two design parameters.

Table 3.3. Breakdown of DP A. Fiber payout unit

Functional Requirement	Design Parameter
A.1. Maintain tension	Passive tensioner
A.2 Allow for quick removal and installation	Quick disconnect
A.3 Minimize inertia	Material selection

The decomposition of the passive tensioner generated two FRs (see Table 3.4).

The MIT/MI discovered that slip-clutches were readily available in various sizes and

torque ratings. Size and hence inertial properties drove the decision process. The final

chosen component was a standard, off-the-shelf item that utilized two high density

polyethylene friction surfaces. These friction surfaces allowed the clutch to disengage

once the tension in the fiber exceeded an adjustable 15-20gram threshold.

Table 3.4. Breakdown of DP A.1. Passive tensioner

Functional Requirement	Design Parameter
A.1.1. Payout fiber once tension exceeds threshold	Slip-clutch
A.1.2. Minimize inertia	Material selection

The second DP for the fiber payout unit resulted with four FRs (see Table 3.5).

These FRs focused on ergonomics, repeatability, and inertia issues. Since the untwisting

spool would be removed and inserted fairly often, the repeatability of the spool's final

position becomes important. A pseudo-kinematic coupling was designed to address this

issue (see Figure 3.7)[19]. Two small ball plungers apply the necessary forces to keep the

spool's shaft registered against the ball-ended pins. The spring constant of both ball

plungers was chosen based on the resulting removal and insertion forces. Figure 3.8

shows the final design of both the pseudo-kinematic coupling and slip clutch.

Table 3.5. Breakdown of DP A.2. Quick disconnect

Functional Requirement	Design Parameter
A.2.1. Low removal force	Frictional force
A.2.2. Low insertion force	Frictional force
A.2.3. High repeatability	Kinematic coupling
A.2.4. Minimize inertia	Material selection

A spring loaded ball plunger
provides restraining force

Ball ends on shaft provide
alignment along axis

Pins with ball ends reference
shaft body using two point
contacts
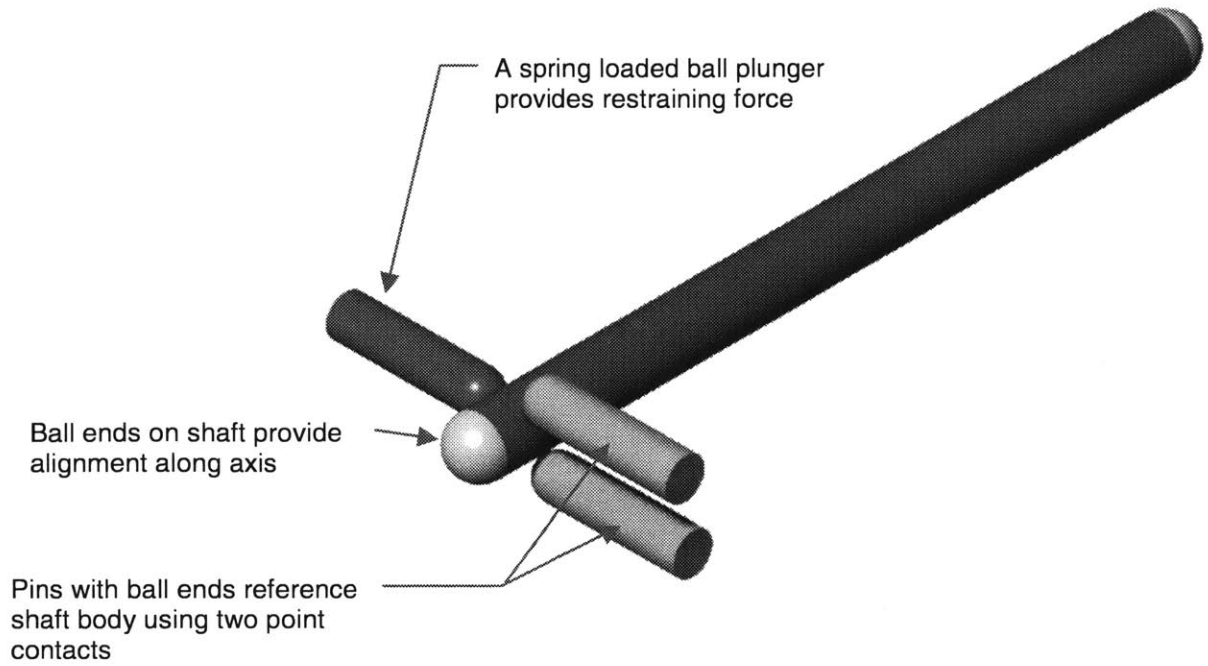
Figure 3.7. A pseudo-kinematic coupling was designed to improve the repeatability of locating the fiber payout unit.

Passive slip clutch

Pseudo kinematic restraint
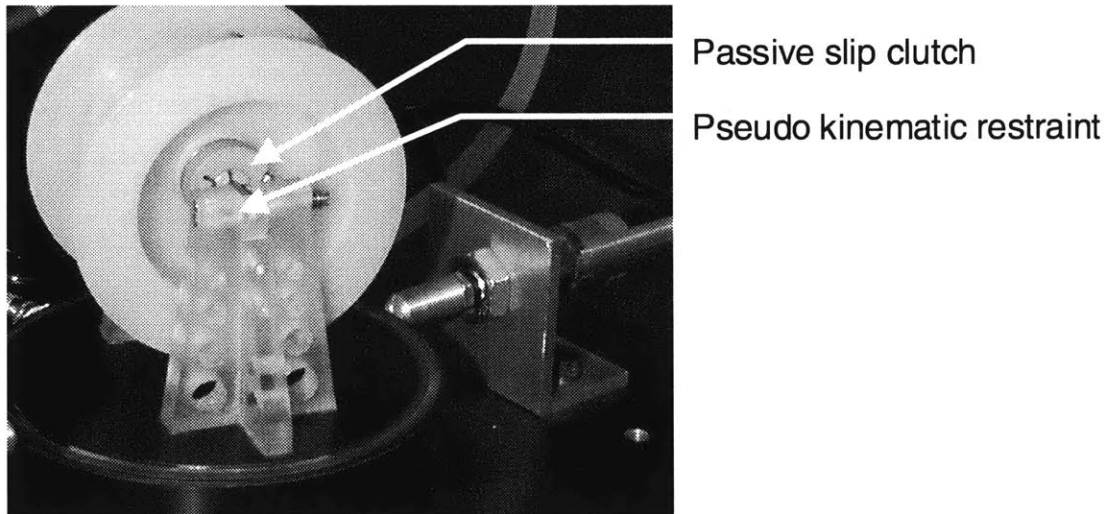
Figure 3.8. Illustration shows final design of the fiber payout unit.

3.3.B. Untwisting subsystem

After completely decomposing the fiber payout unit, the MIT/MI began the decomposition of the untwisting subsystem. Here the three main FRs would allow for rotation, stop rotation, and measure rotation (see Table 3.6). Each of the subsequent DPs was decomposed further into sub-FRs and sub-DPs.

Table 3.6. Breakdown of DP B. Untwisting subsystem

Functional Requirement	Design Parameter
B.1. Allow for rotation	Untwisting bearing
B.2 Stop rotation	Brakes
B.3 Measure twist in fiber - rotation	Encoder assembly

Of the untwisting subsystem DPs, the MIT/MI first decomposed the untwisting bearing (see Table 3.7). This process generated four sub-FRs. The best solution for the associated DPs was a 3" diameter, porous graphite air bearing. This bearing provided virtually frictionless motion in a plane defined by the bearing's surface. This motion was constrained to a purely rotational domain by using a sapphire jewel bearing and pin. This arrangement which is commonly used in analog measurement equipment allowed for a very low rotational friction torque. With an air bearing, the air gap would provide viscous damping, which is a function of velocity (see Equation 3.4). Therefore, at low rotational velocities the associated frictional force is very small.

Table 3.7. Breakdown of DP B.1. Untwisting bearing

Functional Requirement	Design Parameter
B.1.1 Support vertical load	Bearing surface and pressure
B.1.2 Constrain radial motion	Bearing housing design
B.1.3 Provide minimum friction	Static & dynamic friction coefficients

$$\tau = \mu \frac{du}{dy}$$ **Equation 3.4**

where τ = shear stress

μ = viscocity

$\frac{du}{dy}$ = velocity gradient

The brakes constitute the second DP associated with the untwisting subsystem.

Table 3.8 shows a decomposition of DP B.2. Brakes. These brakes are responsible for

arresting the rotating spool as it reaches the equilibrium point. Thus, careful attention

was directed to FR B.2.3. *Do not add rotational disturbance.* Figure 3.9 shows how a flawed

brake design can actually induce a moment. By using brake pads that pivot to create

linear motion, the pads create a small, impulse of torque. This concept was eliminated

and replaced with brake pads that have pure linear translation as shown by Figure 3.10.

The chosen actuator had to be tested for repeatability. A simple experiment was

developed to characterize each pneumatic actuator for its repeatability. Both actuators

could repeat to within 5ms. This time was deemed satisfactory.

Table 3.8. Breakdown of DP B.2. Brakes

Functional Requirement	Design Parameter
B.2.1. Control braking force	Actuator controls
B.2.2. Activate and deactivate brake	Equilibrium time constant
B.2.3. Do not add rotational disturbance	Alignment, geometry, stiffness
B.2.4. Maximize repeatability	Static & dynamic friction coefficients
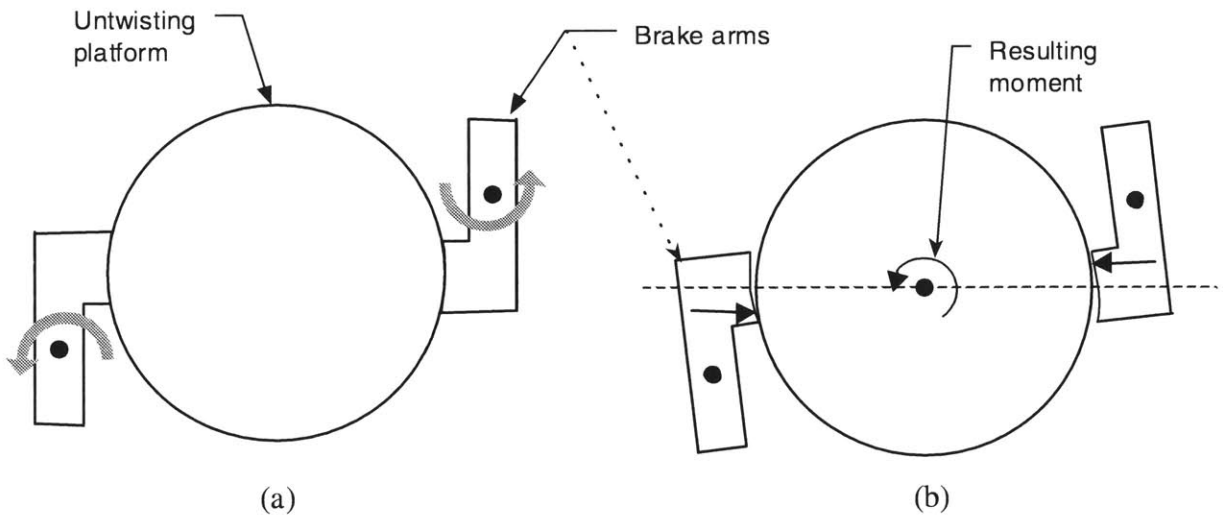
Figure 3.9. As the brakes release (a), one edge of the brake pad disengages contact before the other. This set of off-axis forces results with a moment.
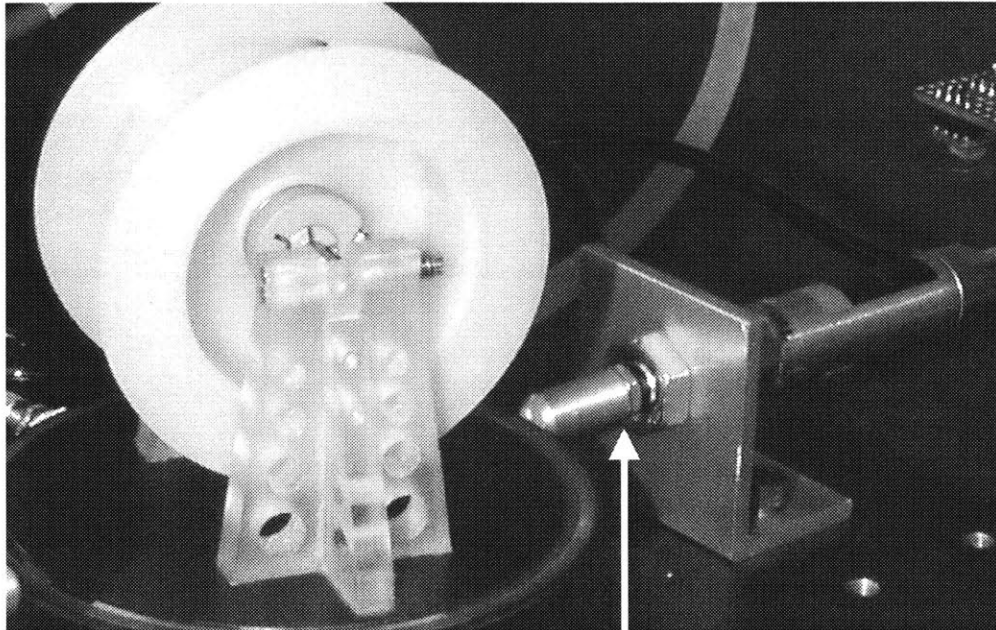
Linear, pneumatic
actuators (opposing one
not shown)

Figure 3.10. Final design of brakes utilize pneumatic
brakes

DP B.2.2. was decomposed further as show in Table 3.9. In order to calculate the

time to first zero-crossing, and the moment the brakes should be applied, one needs to

know the torsional stiffness of a fiber cross-section as well as the untwisting length.

However, minor variations of these parameters from expected values could result a

substantial mis-estimate of the time constant. To eliminate this error, the MIT/MI

decided to calibrate the time constant each time the AFOUM is used (see Table 3.10).

The second FR in Table 3.9 focuses on disturbances to the time constant. One source is

the positional repeatability of the vertical linear stage, e.g. untwisting length. A simple

sensitivity analysis conducted showed that commonly available linear stages had

sufficient repeatability (see Table 3.11).

Table 3.9. Breakdown of DP B.2.2. Equilibrium time constant

Functional Requirement	Design Parameter
B.2.2.1. Calculate time constant	Encoder assembly and software
B.2.2.2. Minimize disturbances	Repeatable discrete length

Table 3.10. Calibration procedure

1. Machine dispenses a known length of fiber
2. User ensures that untwisting platform is at equilibrium
3. Software records current rotational position
4. User displaces untwisting platform some arbitrary angle of rotation
5. Brakes are activated which holds untwisting platform in its displaced position
6. Brakes release allowing untwisting platform to rotate. Simultaneously, the software begins measuring time.
7. Software monitors rotational positional and activates brakes once the recorded position is reached. Simultaneously, the software stops measuring time.
8. The elapsed time is the equilibrium time constant.

Table 3.11. Analysis on how a change in length affects natural frequency (see Appendix C for a derivation of this spreadsheet)

Sensitivity Analysis							
Given:	dL	dL		Length		dT/dL	dT
	in	m		in	m	s/m	s
	0.004	0.0001016		24	0.6096	11.895	0.0012
				36	0.9144	9.712	0.0010
				48	1.2192	8.411	0.0009
				60	1.524	7.523	0.0008
				72	1.8288	6.868	0.0007
				78	1.9812	6.598	0.0007
				84	2.1336	6.358	0.0006
				90	2.286	6.143	0.0006

where dL = change in length

$$dT = \text{change in the period}\left(\frac{1}{\omega_n}\right)$$

The third DP requiring decomposition for the untwisting subsystem was the encoder assembly (see Table 3.12). Satisfying the FRs B.3.2. and B.3.4. was facilitated by the availability of commercially integrated optical sources and sensors capable of precisely reading an encoded surface. The challenging issue with this decomposition was FRs B.3.1. and B.3.3. Most encoder manufacturers utilize small, glass disks with a fine, circular grating deposited on the glass surface. Using a 3″ diameter air bearing created a design constraint which required that measurements occur at the rotary bearings outer perimeter. The optimal solution was to utilize a reflective optical encoder sensor/source with a custom etched encoder disk (see Figure 3.11).

Table 3.12. Breakdown of DP B.3. Encoder assembly

Functional Requirement	Design Parameter
B.3.1. Minimize inertia	Material selection
B.3.2. Generate optical signal	Optical source
B.3.3. Discretize optical signal	Encoder wheel
B.3.4. Sense discrete pulses	Optical sensor

reflective optical encoder

Figure 3.11. Reflective optical encoder mounted on outside edge of untwisting platform.

3.3.C. Fiber take-up subsystem

Finally, the MIT/MI decomposed the last subsystem, the take-up system. This subsystem had four major FRs (see Table 3.13). Since the specific winding pattern on a supply spool is not important, the MIT/MI decided to wind the take-up spool in a helical, winch wind pattern. The second FR focused on controlling tension during the take-up process. Since the take-up system winds untwisted fiber, the third FR emphasizes prevention of twist. Finally, the take-up system has to move along a vertical line as it winds up untwisted fiber; therefore, a vertical, linear stage provides the necessary relative velocity between the take-up spool and fiber. Each of the associated DPs were decomposed further.

Table 3.13. Breakdown of DP C. Take-up system

Functional Requirement	Design Parameter
C.1. Wind in a helical pattern	Coordinate motion between rotary and linear
C.2. Control tension	Tension control mechanism
C.3. Prevent twisting	Velocity differentials
C.4. Provide relative velocity between fiber and spool	Vertical, linear stage

In order to wind in a helical pattern, two types of motion are needed, linear and rotary motions; however, these two movements should be coordinated. Therefore, only one degree of freedom exists. As shown in Table 3.15, coordinating this motion has three associated FRs. The actual coordination of the two motions is done via software. Both the rotary and linear drives are decomposed further into this design methodology.

Table 3.14. Breakdown of DP C.1. Coordinate motion between rotary and linear

Functional Requirement	Design Parameter
C.1.1. Rotate spool	Rotary drive
C.1.2. Move spool axially	Linear drive
C.1.3. Coordinate motion	Software and motion controller

The second DP associated with the take-up mechanism has two FRs as show by Table 3.15. A load cell was added to the design for tension monitoring. A small DC servo motor biased with a constant current controlled the tension via a simple open-loop tension control.

Table 3.15. Breakdown of DP C.2. Tension control mechanism

Functional Requirement	Design Parameter
C.2.1. Measure tension	Load cell
C.2.2. Adjust tension	DC motor operating in current mode

Next, DP C.3. *Prevent twisting* was decomposed into two FRs (see Table 3.16). The first FR focuses on velocity gradients. Figure 3.12 illustrates this point. A fiber strand being wound onto a mandrel with flanges moves with ω^*r tangential velocity. If this strand were to contact a flange wall, that fiber section would see a tangential velocity component that could induce twist. Thus, DP C.3.1. emphasizes the need to avoid contact with vertical walls. The second FR describes the need to minimize the number of contact points a fiber section sees. Since a flat pulley can induce twist as discussed for the drawing capstan in Chapter 2, all pulleys on the AFOUM have vee-grooves.

Table 3.16. Breakdown of DP C.3. Prevent twisting

Functional Requirement	Design Parameter
C.3.1. Minimize velocity gradients	Avoid contact with vertical walls
C.3.2. Minimize number of contact points	Two contact points
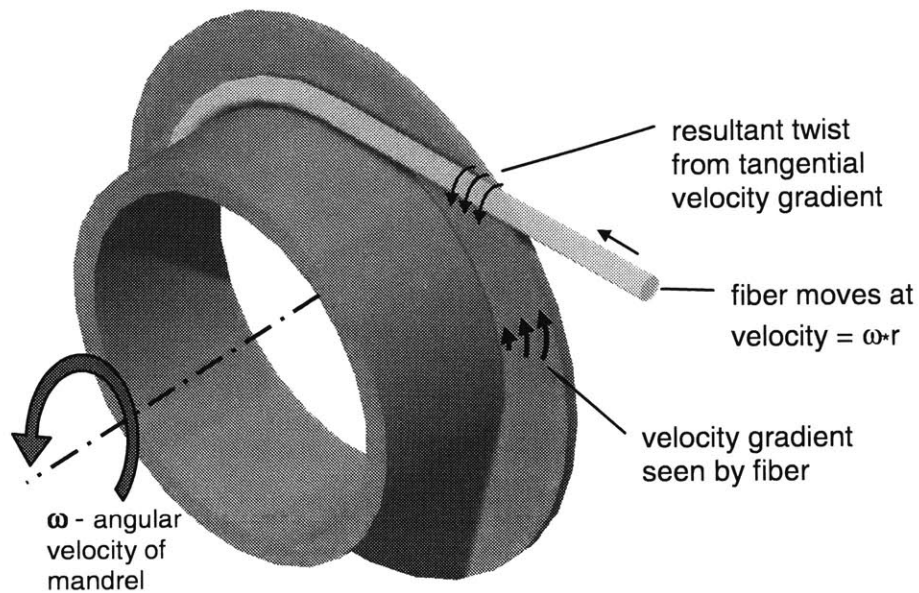
Figure 3.12. A turn of fiber near a vertical flange will see velocity gradient. This could lead to twist.

The final DP, *Vertical, linear stage*, was decomposed into three sub-FRs. FR C.4.1. established that the linear stage should interface with the take-up assembly in order to provide relative motion between the take-up spool and fiber. Furthermore, FR C.4.2. suggests that holding torque becomes a concern. This was addressed with proper motor sizing and gear reduction. Finally, the last FR reiterates the importance of position repeatability; this point was discussed earlier (see Table 3.11).

Table 3.17. Breakdown of DP C.4. Vertical, linear stage

Functional Requirement	Design Parameter
C.4.1. Move spool relative to fiber	Interface to take-up assembly
C.4.2. Maximize position repeatability	Equilibrium time constant sensitivity
C.4.3. Support take-up assembly	Holding torque

A decomposition of DP C.1.1. resulted with three sub-FRs. In order for the rotary drive to support a take-up spool, a spool hub had to be designed. Also, the MIT/MI decided that a small DC servo motor could provide the necessary torque to control the fiber's tension.

Table 3.18. Breakdown of DP C.1.1. Rotary drive

Functional Requirement	Design Parameter
C.1.1.1. Support spool	Spool hub
C.1.1.2. Provide torque	DC servo motor
C.1.1.3. Control torque	Torque command signal

DP C.1.2. decomposed into five sub-FRs (see Table 3.19). The first function of the linear drive involved supporting the rotary drive. This was accomplished with a bracket that clamped onto the rotary actuator's body. The other end of the bracket had to attach to the linear stage through existing mounting holes. Also, the linear drive had to attach to the vertical stage; thus, a mounting plate had to be designed. The MIT/MI decided that a readily available leadscrew driven stage would provide the needed horizontal displacement.

Table 3.19. Breakdown of DP C.1.2. Linear drive

Functional Requirement	Design Parameter
C.1.2.1. Support rotary drive	Rotary support bracket & load capacity
C.1.2.2. Attach to rotary support bracket	Fasteners through existing mounting holes
C.1.2.3. Attach to vertical stage	Mounting plate
C.1.2.4. Provide horizontal displacement	Leadscrew driven stage – DC servo motor
C.1.2.5. Control displacement	Displacement command signal

DP C.1.3. lists the necessary sub-FRs in order to coordinate the motion between the rotary and linear drives (see Table 3.20). First, a rotary encoder and digital counter would have to measure the angular position of the take-up spool. Next, the software would calculate the desired linear position. This process would result with coordinated motion between the two axes, which would result with a helical wind. Figure 3.13 shows the final design of the take-up subsystem.

Table 3.20. Breakdown of DP C.1.3. Software and motion controller

Functional Requirement	Design Parameter
C.1.3.1. Measure angular position	Rotary encoder & motion controller board
C.1.3.2. Calculate linear position as function of angular position	Software

Coordinated motion between take up spool and x-axis

Vee grooves on pulleys
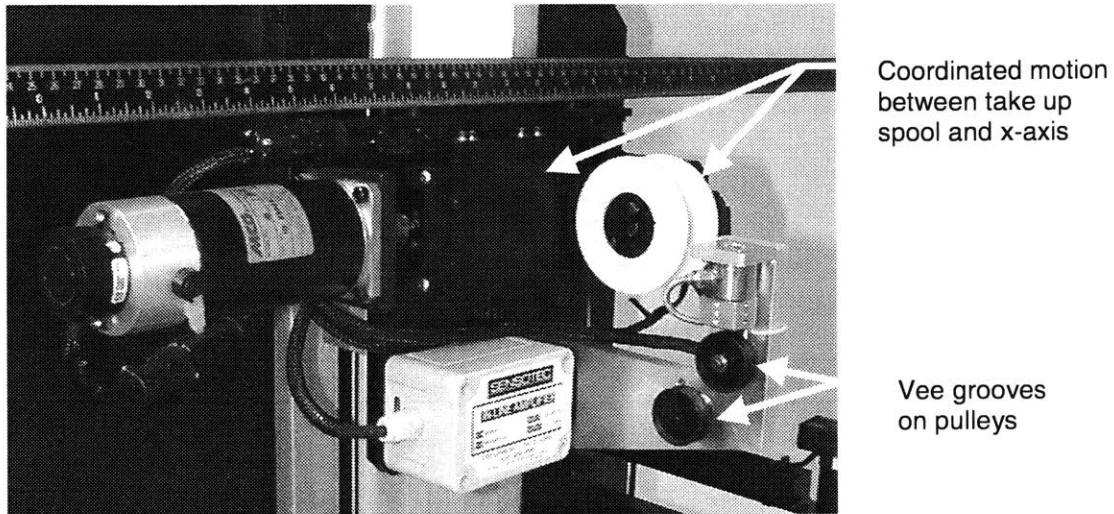
Figure 3.13. Final design of the take-up subsystem.

The next high level DP, D. *Transfer winder* was decomposed as shown in Table 3.21. A threaded shaft was used to support the manufacturer's spool. Tapered spool lock nuts secured a manufacturers spool to the shaft, while the taper adapted to various diameter fiber spools including the coil winder's supply spools. Tension was applied by biasing a DC motor with a constant current. An encoder mounted on the same shaft as an idler pulley was used to measure the length of fiber transferred.

Table 3.21. Breakdown of DP D. Transfer winder

Functional Requirement	Design Parameter
D.1. Support manufacturer's spool	Shaft
D.2. Lock spool to shaft	Spool lock nuts
D.3. Accept different size spools	Taper on spool lock nuts
D.4. Provide tension	DC motor
D.5. Measure length	Length measuring encoder

78

The final high level DP, E. *Safety features,* was decomposed (see Table 3.22). The first FR *Limit tension level* describes the need for careful restriction of high tensions. If a strand of fiber experiences high tension, the jacket could be damaged that could compromise polarization performance or in extreme case even break the fiber. To eliminate this risk, the supply spool motor's proportional gain, Kp, was purposely kept low. This created a servo-spring effect. In software, adjusting the maximum position error allowable reduced the travel of this virtual spring. This feature is especially necessary for a transfer wind operation.

Table 3.22. Breakdown of DP E. Safety features

Functional Requirement	Design Parameter
E.1. Limit tension level	Position error detection
E.2. Prevent vertical axis from falling	Vertical axis brake

Before the AFOUM, a transfer wind was typically performed by hand (using two reels supported on two shafts). This would wind fiber onto a spool in a very uneven manner. If this same spool was placed onto the AFOUM for a transfer wind, an operator would have to maintain a vigilance for dangerous fiber geometry that could lead to breakage. Therefore, by implementing a soft servo spring with a low position error, the machine can automatically stop when appropriate.

The second safety feature incorporated into the AFOUM was a vertical axis brake. This brake ensured that the vertical axis would remain fixed when the machine was powerless. Otherwise, the take-up subsystem could slowly creep downward.

The design of the AFOUM has listed a detailed characterization of functional requirements and design parameters. This process allowed for the necessary

79

procurement of essential components. The next phase involved the creation of a user interface and control software.

3.4. Software design

A computer running custom C++ software controls the entire machine (all electronics and motors). Through this interface, a user can control all of the various machine functions. In addition, the program can store important information in text files such as twist data.

The user interface was programmed in C++ and run in a DOS environment for several reasons. The most important justification was to make an interface that was similar to the coil winder. This way the coil winder's operator could learn to run the untwisting machine without an extensive training period. This decision allowed the use of the coil winder program's source code as a reference, greatly shortening development time. Furthermore, by using C++, revisions to the untwisting machine's code were easily made.

An important feature of the untwisting machine's program includes the ability to save position and untwisting parameters into a text file. This action eliminates the need for rehoming each axis after shutting down the program; an action that normally would erase all position information. In addition to position, untwisting parameters like the fixed length and tension are also saved to the same text file. Upon initialization, the program loads these saved values from the text file.

Another important feature of the untwisting machine's program is the ability to record twist data. This provides valuable information to the user who can use this data to evaluate the quality of manufacturers products as delivered on spools. Like the

position of each axis, the program saves twist data to a text file after completing each

untwisting operation. The saved data comprises two fields: total length untwisted (e.g.

fiber position) and an accumulated angle from an initial zero. This angle is a cumulative

twist. It is not reset after each untwisting operation. More details concerning twist data

will be presented in Chapter 4.

CHAPTER 4   EVALUATION OF AN UNTWISTING MACHINE

After completing the design and construction of the AFOUM, the next phase involved a detailed validation process to document the AFOUM's capabilities. Furthermore, several experiments provided valuable information concerning the extent that one can elastically untwist optical fiber.

4.1.   *Confirmation of twist removal*

A simple experiment verified the untwisting process. A test strand of fiber was twisted by a known amount. Then the AFOUM processed this test specimen three times. Figure 4.1 verifies that four turns of twist were intentionally introduced into the fiber. Note that this graph indicates the accumulated amount of twist present at various points along the fiber.   After the first pass, a very small amount of apparent twist remains; interestingly, after the second pass the same residual amount of twist still remains (see Figure 4.2). This repeatable amount of twist was further investigated.
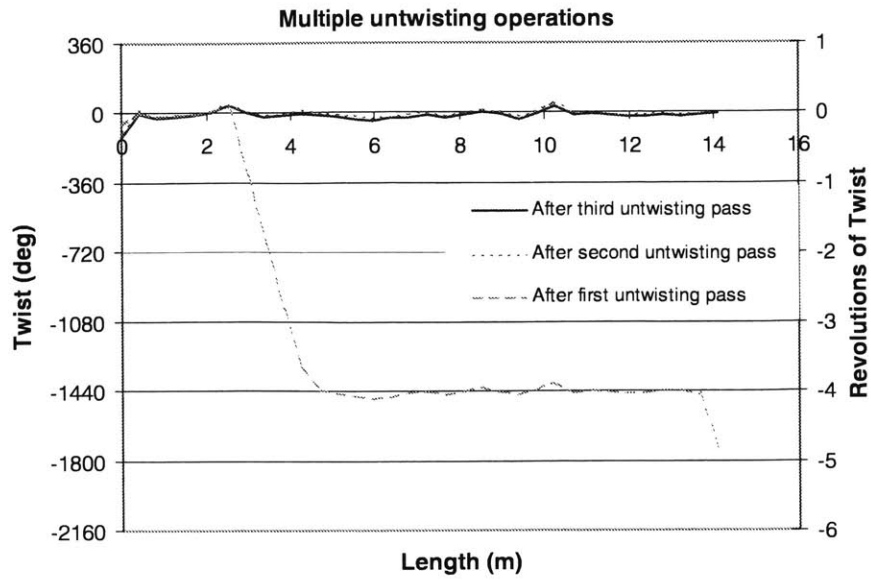
Figure 4.1. Twist was intentionally added to a 14m section of fiber. The first untwisting pass shows that approximately 4 turns of twist was added. The second and third passes confirm that the twist was removed.
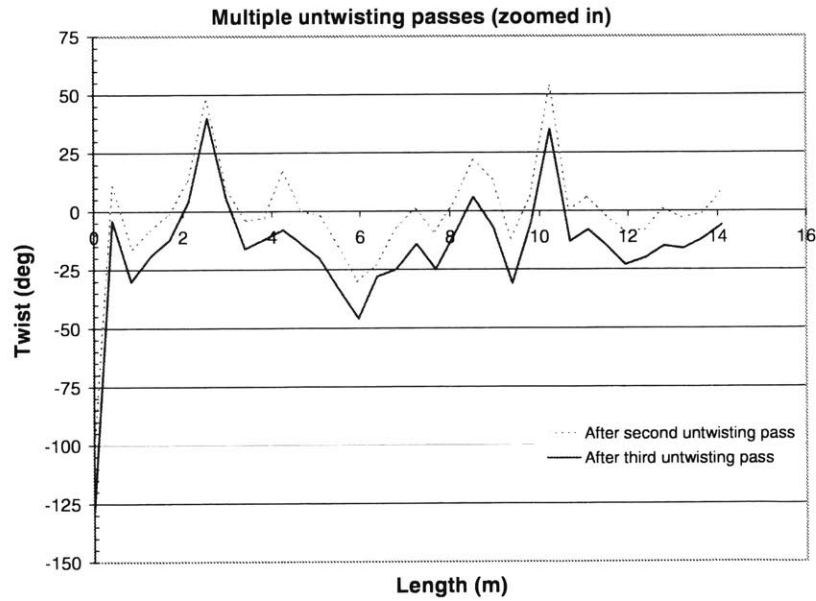

Figure 4.2. A zoomed in view of the second and third untwisting passes shows that the amount of residual twist is repeatable.

This could be explained by two possible hypotheses. First, the untwisting

machine itself induces twist into the fiber. If this was indeed correct, then the apparent

residual twist spectrum should contain a frequency component that resembles a

characteristic length on the AFOUM. After a careful study of the twist data, no

conclusive evidence linked fiber handling components on the AFOUM to the torsional

strain.

The second hypothesis is that torsional strain arises from asymmetric elasticity of

the polymer/glass composite fiber. As shown in Equation 4.1, if a material has a non-

zero element in its stiffness matrix, an applied longitudinal stress could produce a

torsional strain about one of the principal axes. For example, if the constant S_{14} is non-

zero, then an applied stress σ_1 would result in a shear strain γ_{23} in the plane normal to

that stress. Jones discusses such properties of anisotropic materials [20]. Therefore, the

result in Figure 4.2 implies that the right half of the constant matrix is non-zero.

$$
\begin{bmatrix}
\varepsilon_1 \\
\varepsilon_2 \\
\varepsilon_3 \\
\gamma_{23} \\
\gamma_{31} \\
\gamma_{12}
\end{bmatrix}
=
\begin{bmatrix}
S_{11} & S_{12} & S_{13} & S_{14} & S_{15} & S_{16} \\
S_{21} & S_{22} & S_{23} & S_{24} & S_{25} & S_{26} \\
S_{31} & S_{32} & S_{33} & S_{34} & S_{35} & S_{36} \\
S_{41} & S_{42} & S_{43} & S_{44} & S_{45} & S_{46} \\
S_{51} & S_{52} & S_{53} & S_{54} & S_{55} & S_{56} \\
S_{61} & S_{62} & S_{63} & S_{64} & S_{65} & S_{66}
\end{bmatrix}
\cdot
\begin{bmatrix}
\sigma_1 \\
\sigma_2 \\
\sigma_3 \\
\tau_{23} \\
\tau_{31} \\
\tau_{12}
\end{bmatrix}
\qquad \textbf{Equation 4.1}
$$

The next experiment tests the second hypothesis and verifies the conclusion of

the first hypothesis. Using the same strand of fiber as used before, the strand was

inverted (end for end) and reprocessed using the AFOUM. If the second hypothesis is

correct, then the torsional strain would mirror the previous experiments. On the other

hand, if the twist data continued to show a resemblance to the original data, then the first hypothesis could still be valid. As shown in Figure 4.3, the dotted line represents the torsional strain after inverting the fiber strand. Figure 4.4 plots the inverted data in reverse order for comparison purposes, i.e. with fiber stations matched. The correlation of peaks and dips suggests that off-diagonal stiffness matrix values vary down the length of the fiber, and that they have a governing role in dictating small angle rotational strain of the fiber. Further, this suggests that the use of the AFOUM for untwisting will leave residual twist "noise" unless the fiber elasticity was perfectly regular down its length. From these two graphs, one can conclude that the apparent twist in the fiber is actually from the fiber jacket undergoing a torsional strain and not induced by the AFOUM. Therefore, this limits the resolution of the AFOUM's elastic untwisting capabilities to approximately ±25 degrees. Further characterization of this strain behavior was considered outside of the scope of this thesis.
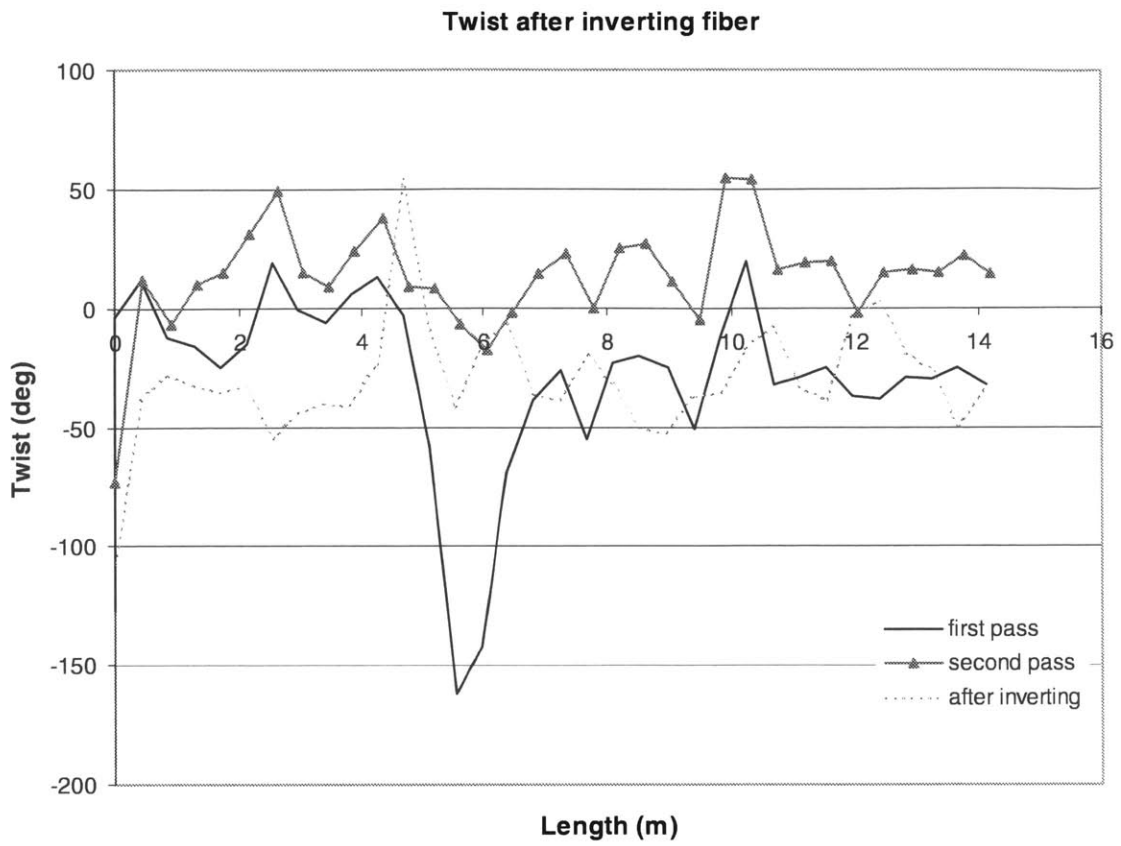
Figure 4.3. After inverting the fiber end for end, the twist profile is essentially a mirror of the second pass. In this plot, the first pass was performed to ensure that twist-free fiber was being tested during the second and subsequent passes.

Twist after inverting fiber

Inverted case is plotted in reverse order
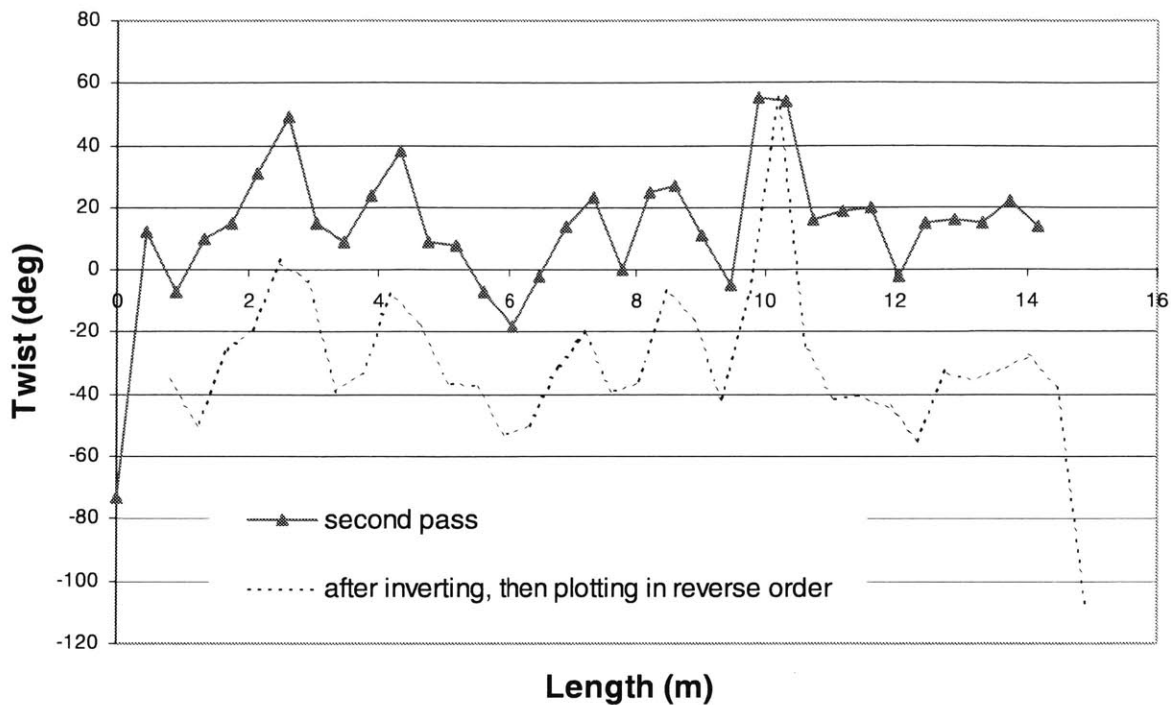
Figure 4.4. For comparison purposes, the inverted fiber's twist profile is plotted in reverse. The inverted fiber's twist profile closely matches the second pass' profile. The offset is due to a different starting location.

4.2. Untwisting 622m

The AFOUM ran its first automated run on 622m of fiber. Not only was the AFOUM used to untwist the fiber, it was also used to transfer the appropriate amount of fiber from spool to spool. Useful and surprising data was gathered during the untwisting operation.

Figure 4.6 shows twist data collected from this 622m sample. Several observations were made. First, the twist had average peak to peak cycles at 64m

intervals. Also, each peak contained an average of ±8 revolutions of twist. Furthermore, the average width of each peak was 30m. Due to a lack of information from fiber manufacturers, no conclusions were made as to the sources of these peaks.

The twist data in Figure 4.6 shows a peculiar overall trend. The twist appears to drift at about 7 degrees per meter. A thorough analysis of the twist measuring encoder determined that the drift was due to an incorrect standoff spacing specification (see Figure 4.5) having been given in the optical encoder manufacturer's data sheet. After corroborating with the manufacturer, the correct standoff value was determined and implemented. This correction eliminated any measurable amount of drift in the twist measuring encoder.
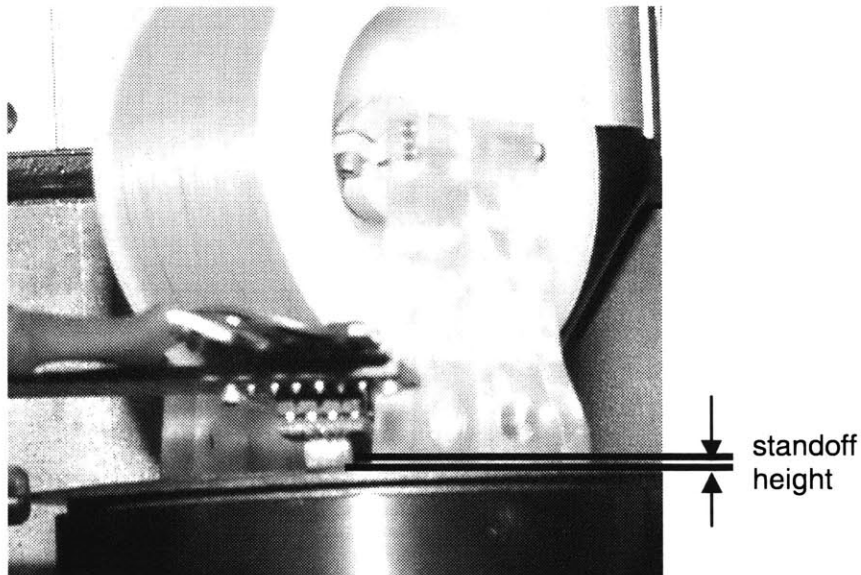
Figure 4.5. An incorrect standoff value in the manufacturer's data sheet led to a rotational drift of 7 degrees per meter.

Measured Twist

Figure contents:

- Y-axis label: Twist (deg)
- Y-axis values: 1000, 0, -1000, -2000, -3000, -4000, -5000, -6000, -7000
- X-axis values: 0, 100, 200, 300, 400, 500, 600, 700
- X-axis label: Length of Fiber (m)

Twist = -7.2*(Length) - 1723.6

Averages for each peak
twist = ± 8 revolutions
peak to peak = 64m
width of each peak = 30m
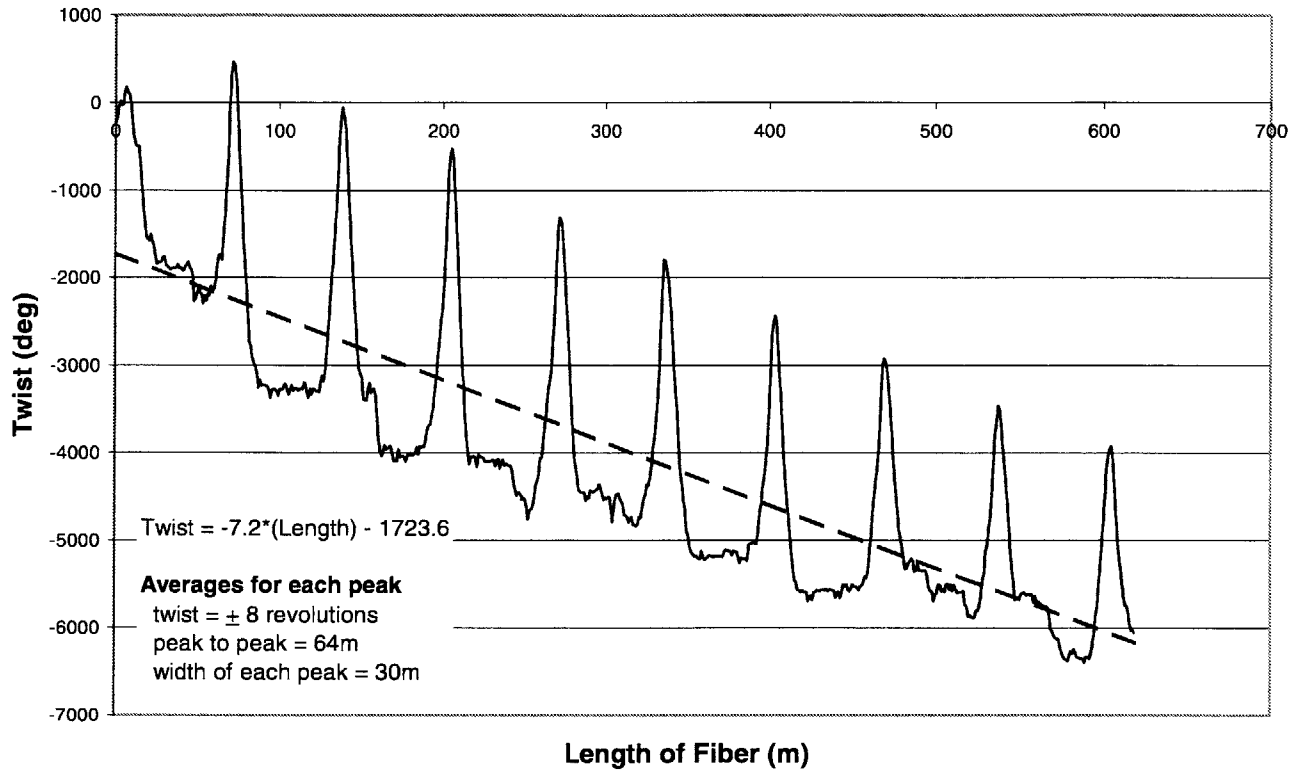
Figure 4.6. Twist data collected from 622m of fiber.

4.3. Reducing winding errors on coil winder

Draper Laboratory used this untwisted fiber to wind a FOG coil. Traditionally, a coil pack would begin to experience more winding errors as the number of layers increased; however, by using the untwisted fiber, virtually no errors appeared in mid-wind on any particular layer. The coil winding machine could wind from one flange to the other with little or no user intervention. This was considered an enormous improvement in both FOG quality and process time.

CHAPTER 5   FUTURE WORK

As mentioned in Chapter 1, one attribute of a high performance gyro includes minimizing the sensitivity to the Faraday effect. Undesirable drift can be eliminated if a PM fiber's polarization field does not have a twist spectral component equivalent to one turn of fiber on the mandrel. Therefore, this chapter discusses a proposed method for detecting the orientation of a PM fiber's polarization field and actively reorienting the fiber cross-section to reduce effects from the Faraday effect.

5.1.   *Optical Untwisting*

Two general methods were considered to detect the orientation of the polarization field. The first method attempts to utilize photoelasticity to visualize the stress within the cladding to infer the orientation. A more direct approach relies on optical diffraction.

5.1.A. Photoelasticity

When elastically deformed, the optical properties (e.g. index of refraction) of a photoelastic specimen become anisotropic. Using a special optical system and polarized light, the stress distribution within the specimen may be deduced from interference fringes that are produced. An example of this technique is illustrated in Figure 5.1.

This technique assumes that the rotated polarization field is stressed. This may not be true if the fiber has experienced room temperature creep. In that case, there would be no correlation between orientation and stress. Thus, another method had to be explored.
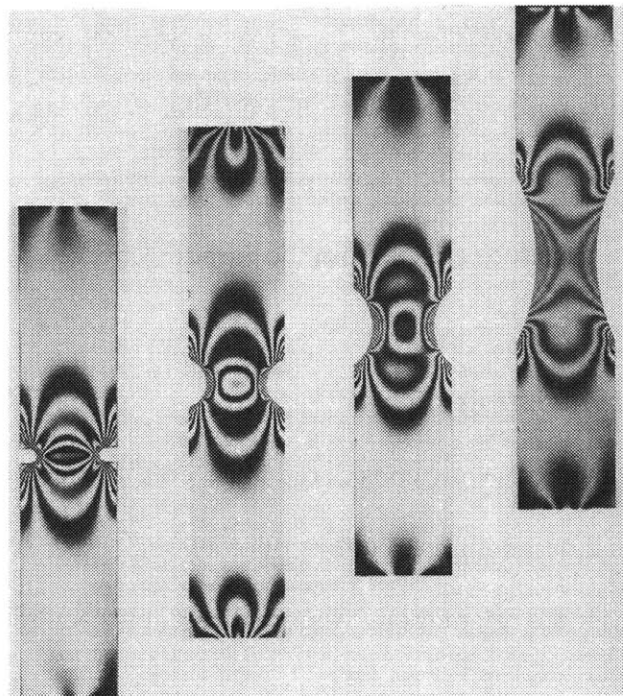
93

Figure 5.1. The four notched and transparent rods shown in this photograph demonstrate the phenomenon of photoelasticity. These fringes within the four photoelastic specimens shown in the photograph indicate how the stress concentration and distribution change with notch geometry for an axial tensile stress. [21]

5.1.B. Optical diffraction

An alternative method relies on optical diffraction. This proposed arrangement originates from a basic two-slit optical experiment shown in Figure 5.2. As a plane wave passes through a double slit, a series of reinforcement and cancellation waves produce a diffraction pattern. As shown in Figure 5.3, the spacing between reinforced areas is a function of the slit width and wavelength as derived from Fourier optics [22]. A fiber's cross-section has some similarity to this classic optical experiment. The two stress rods in type 2 PM fiber, typically used for gyros, have a different index of refraction from the rest of the cladding. Therefore, as the cladding rotates through 90 degrees, the changes in index of refraction mimic a classic two slit experiment (see Figure 5.4).
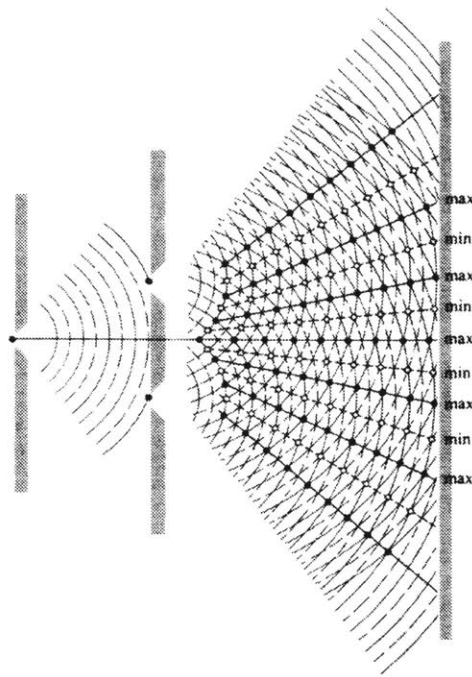
Figure 5.2. Classic two slit optical experiment demonstrates the principle of cancellation and reinforcement [22].

(a)   (b)
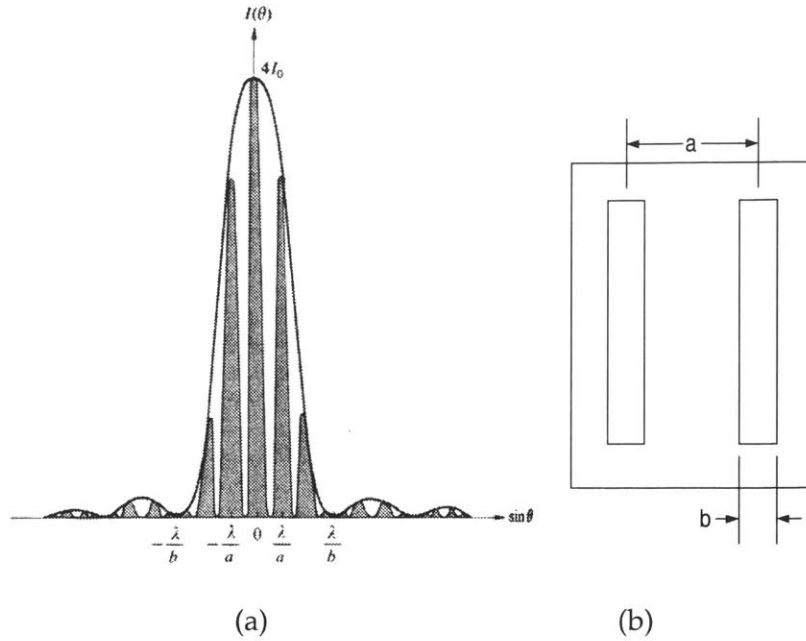
Figure 5.3. Spacing of diffraction pattern (a) is function of slit spacing and width (b) [22].

(a)   (b)

Figure 5.4. When the stress rods are oriented along the HeNe's path (a), the slit spacing is essentially zero. After rotating the cladding 90 deg. (b), the slit spacing becomes a maximum equal to distance separating the two stress rods.

The MIT/MI gathered experimental data that proved a HeNe laser beam passing transversely through a PM fiber could indeed generate a diffraction pattern (see Figure 5.5). Also, the spacing between the projected fringes varied as the PM fiber was rotated; however, there was no confirmation that maximum diffraction sp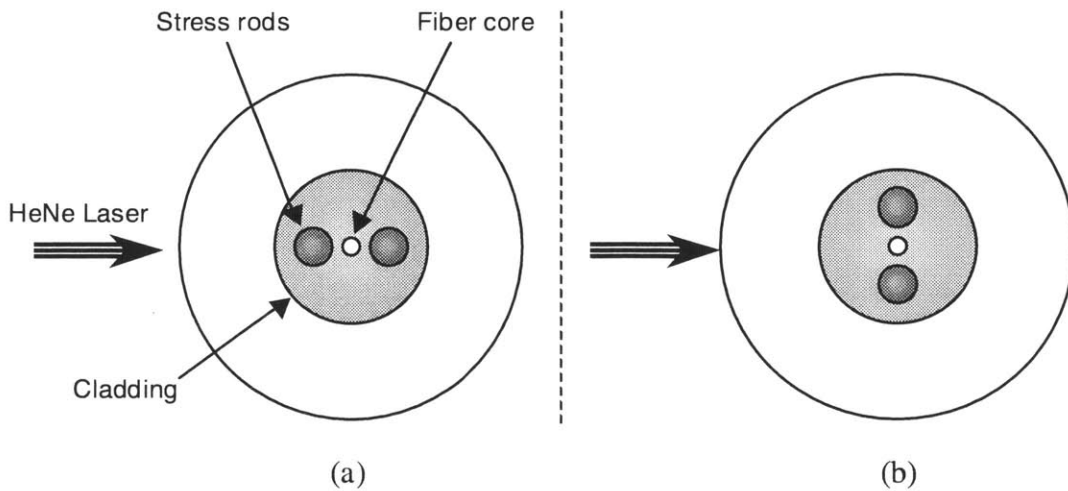acing correlated with minimum spacing between stress rods. The MIT/MI used these results to formulate a process for optical untwisting.
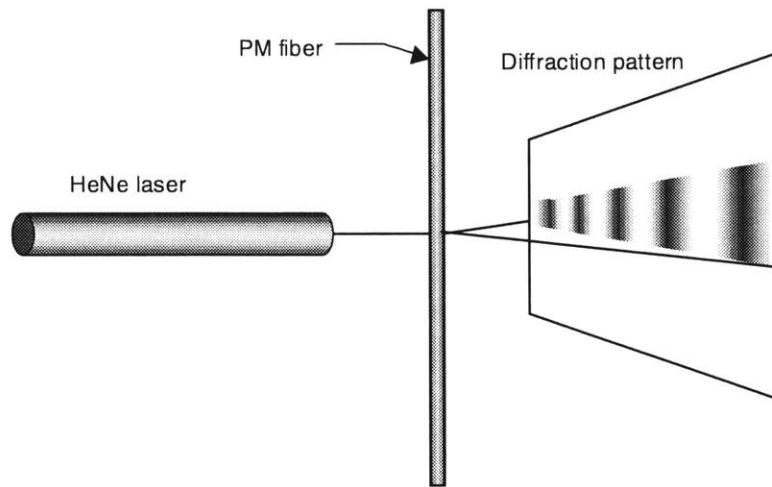
Figure 5.5. This experimental setup proved that a HeNe laser passing traversely through a PM fiber cross-section could indeed generate a diffraction pattern.

An optical untwisting apparatus as a first step would eliminate elastic torsion in the fiber by utilizing the existing AFOUM. However, the take-up process used by the AFOUM would require modification. A diffraction based measurement station near the take-up spool would measure the stress rod orientation. A position signal would be fed back to a rotary stage that supports the pneumatic brakes (see Figure 5.6). Using servo control, the entire untwisting spool assembly would be rotated to achieve the desired stress rod orientation. Next, a take-up spool can wind the fiber.
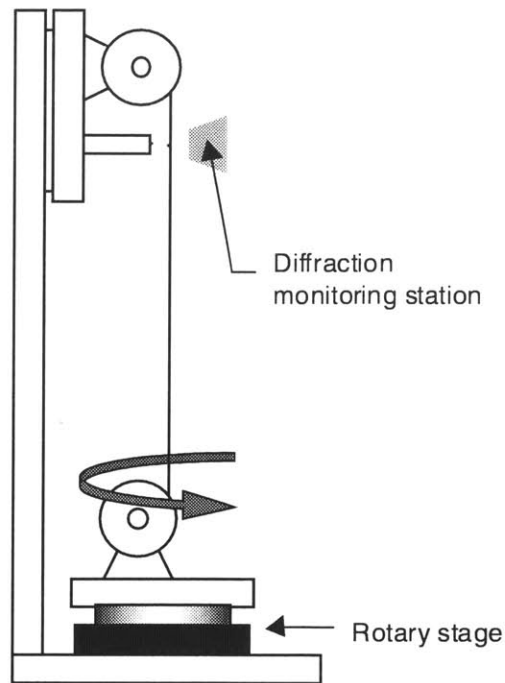
Figure 5.6. Modifications to the AFOUM for optical untwisting include a diffraction monitoring station and a rotary stage.

5.2. Stress relieving

One should note that because the geometric and elastic principal axes of a given piece of fiber are unlikely to coincide, rotating the fiber body to zero geometric strain would likely induce elastic strain energy that create the winding errors described earlier. To relieve this torsion, the entire take-up spool could be subjected to a stress relieving process such as annealing that would relax the strain axes toward the geometric axes. This process assumes that the strained fiber wound on the take-up spool does not shift over time. With sufficient tension and friction, shifting should not occur.

CHAPTER 6 CONCLUSIONS

As mentioned in Chapter 1, three main coil parameters affect a high performance FOG: first, the Shupe effect due to a moving temperature gradient, second, the Faraday magnetic effect scatter, and finally, bias drift related to polarization scatter. By lowering coil winding tensions, polarization cross-talk can be significantly reduced.

Several issues arise during a low tension wind, including some significant fiber positioning errors caused by small radii of curvature and elastic twist in the fiber. After a thorough investigation, several sources of elastic twist were identified; the largest one was hypothesized to originate from the fiber manufacturing process. Since eliminating twist during the manufacturing process requires access to proprietary information, Draper and the MIT Manufacturing Institute (MIT/MI) decided to pursue the development of an experimental untwisting process.

The first step in eliminating twist was to apply the fundamentals of mechanics to model torsional strain in fiber. This model led to the development of a simple, open loop untwisting process. The next step involved decomposing the chosen untwisting process into a hierarchy of functional needs and design parameters. These three steps created the Automated Fiber Optic Untwisting Machine (AFOUM) as shown in Figure 6.1.

Several experimental trials confirmed the AFOUM's ability to remove twist. The verification process was initiated with imparting a known twist angle into a length of optical fiber, which was subsequently processed by the AFOUM. Data generated by the untwisting process revealed that the known twist angle was removed while leaving a small quantity of residual torsional strain. This twist "noise" was shown to be torsional

99

strain caused by non-zero off-diagonal terms of the fiber's stiffness matrix. Thus, the AFOUM's untwisting resolution is limited to ±25 degrees.

The first coil wound with untwisted fiber used 622m of optical fiber. Data produced by the AFOUM showed that this particular batch of fiber had periodic peaks with a peak height of ±8 revolutions of twist spaced at approximately 64m. Data taken during this untwisting operation marked the first time that a fiber's twist history was recorded.

The untwisted fiber significantly reduced the number of winding errors at low tensions. As mentioned earlier, the coil winder's operator could wind an entire layer without any mid-wind, manual interventions. This dramatically reduced the overall coil winding time and undocumented applications of force from each manual intervention.

As a recommendation for future work, this thesis suggests modifications in the form of additional equipment that would allow the reduction of another significant error term, the Faraday effect. During the early design phase, special features were integrated into the AFOUM so that additional sensors and positioning devices can be easily integrated to the as-built hardware.

The AFOUM has become a valuable tool for measuring and preparing fiber for the coil winder. In addition, staff members not associated with the coil winder welcome the AFOUM's capability to accurately measure long lengths of fiber. This feature alone will undoubtedly be used as an independent capability. In conclusion, the development of the AFOUM has enabled better monitoring of fiber quality and incremental improvements in FOG performance.
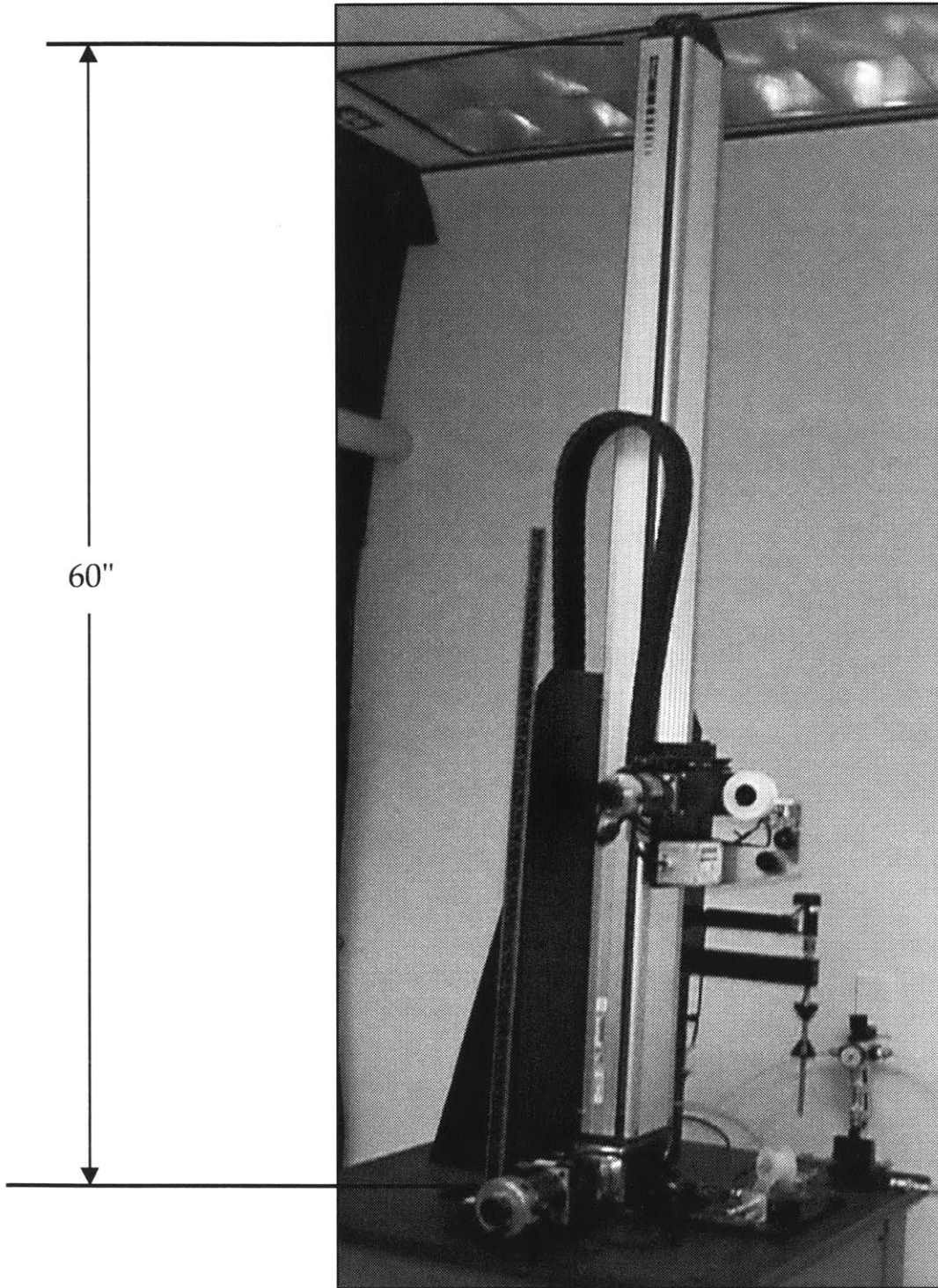
Figure 6.1. The fully assembled AFOUM stands approximately 9 feet tall and can untwist 5 feet of fiber with each pass.

BIBLIOGRAPHY

1.   Lawrence, A., *Modern Inertial Technology: Navigation, Guidance, and Control*. 1993, New York: Springer-Verlag. pp. 4-5, 84-85.

2.   Crandall, et al., *Dynamics of Mechanical and Electromechanical Systems*. 1982, Florida: Robert E. Krieger Publishing Company. pp. 238-246.

3.   Wrigley, H. and Denhard, *Gyroscope Theory, Design, and Instrumentation*. 1969, Cambrige, MA: The MIT Press. pp. 4-5.

4.   Tsai, M.-H., *Experimentation, Characterization and Enhancement of an Automated Fiber Optic Gyroscope Coil Winding Machine*, MS in Mechanical Engineering. 1998, Massachusetts Institute of Technology: Cambridge.

5.   Nauck, L.M.H., *Fiber-Optic Gyroscopes. History, Theory, and Application to Navel Systems*. Multi-Redcom Technical Training Session, 1997, pp. 10-11.

6.   Lin, S.M., *Design and Development of an Automated Fiber Optic Gyroscope Coil Winding Machine*, MS in Mechanical Engineering. 1997, MIT: Cambridge.

7.   Dakin and Culshaw, *Optical Fiber Sensors Applications, Analysis, and Future Trends*. Vol. 4. 1997, Norwood, MA: Artech House. pp. 197.

8.   Sagnac, G., *L'ether lumineux demontre par l'effet du vent relatif d'ether dans un interferometre en rotation uniforme*. C. R. Acad. Sci., 1913. 95: pp. 708-710.

9.   Ezekiel, S. and H.J. Arditty, *Fiber-Optic Rotation Sensors. Springer series in optical sciences*. Vol. 32. 1982, New York: Springer-Verlag. pp. 2-26.

10.   Davis, J.L., *Inertial Rotation Sensing Using a Fiber Optic Sagnac Interferometer*, PhD in Electrical Engineering. 1981, MIT: Cambridge.

11.   Vali, V. and R.W. Shorthill, *Fiber Ring Interferometer*. Applied Optics, 1976: pp. 15, 1099.

12.   Shupe, D.M., *Thermally induced nonreciprocity in the fiber-optic interferometer*. Optical Society of America, 1980. 19(5): pp. 654-655.

13.   Baron, H. and e. al. *RPM Measuring Device Utilizing an Optical Fiber Coil and Winding Method for Making the Coil*, United States Patent, 4,781,461

14.   Ltd., L.S.C. *Fiber Optic Sensing Coil*, United States Patent, 4,793,708

15.   Cogdell, J.R., *Foundations of Electrical Engineering*. 1990, New Jersey: Prentice Hall. pp. 667.

16.   Hotate, K. and K. Tabe, *Drift of an optical fiber gyroscope caused by the Faraday effect: influence of the earth's magnetic field*. Applied Optics, 1986. 25(7): pp. 1086-1092.

17.   Lenders, W.L., *The Orthocyclic Method of Coil Winding*. Phillips Technical Review, 1962. 23: pp. 365-404.

18.   Gere, J.M. and S.P. Timoshenko, *Mechanics of Materials*. 1990, Boston: PWS Publishing Company. pp. 252, 461-464.

19.   Slocum, A.H., *Precision Machine Design*. 1992, New Jerey: Prentice Hall. pp. 401-408.

20.   Jones, R.M., *Mechanics of Composite Materials*. 1975, New York: McGraw-Hill Book Company. pp. 355.

21.   Measurements Group, *What is Photoelasticity*. March 1999: Raleigh, North Carolina, http://www.measurementsgroup.com/first/pe.htm [cited on March 1999].

22.   Hecht, E., *Optics*. 1987, Reading, MA: Addison-Wesley Publishing Company. pp. 407-408.
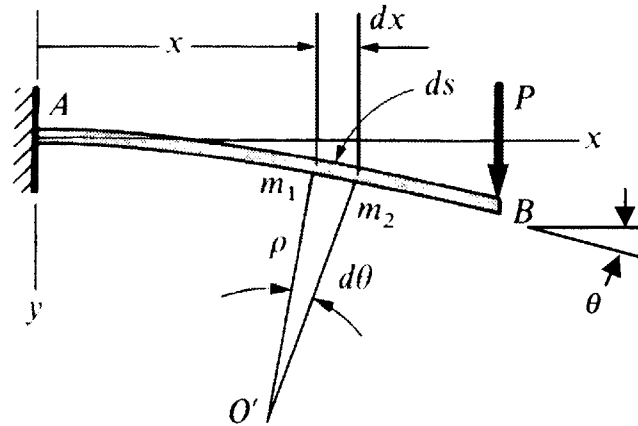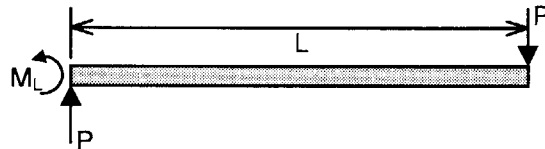
104

APPENDIX A: RADIUS OF CURVATURE

Figure A. Curvature of a bent beam caused by a point load.
Photo courtesy of Gere and Timoshenko [18].

Gere and Timoshenko give the standard beam deflection equation as:

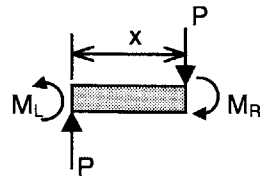$$\frac{\partial^2 v}{\partial x^2} = \frac{M}{EI}$$

Derive the moment expression, M, as a function of x:

From an equilibrium moment balance

$$M_L = PL$$

Now take a slice at some arbitrary x:

From an equilibrium moment balance

$$M_R = M_L - Px = P(L - x)$$

Now, integrate the standard beam deflection equation:

$$\int \frac{\partial^2 v}{\partial x^2} = \int \frac{M}{EI} = \int \frac{P(L-x)}{EI}$$

$$\frac{\partial v}{\partial x} = \frac{P\left(Lx - \frac{x^2}{2}\right)}{EI} + A$$

since $\frac{\partial v}{\partial x}(0) = 0$, $A = 0$

Note that the slope of the deflection curve is given by the derivative:

$$\frac{\partial v}{\partial x} = \frac{dy}{dx} \quad \therefore \frac{dy}{dx} = \frac{P\left(Lx - \frac{x^2}{2}\right)}{EI}$$

In this case, the slope is the angle of the deflected beam at some position x along the beam.

$$\frac{dy}{dx} = \delta' = \theta = \frac{Px}{2EI}(2L - x)$$

Taking the derivative of this term gives us:

$$\frac{d\theta}{dx} = \frac{P(L-x)}{EI}$$

Assuming that the deflection is small, then dx ~ ds. Now the radius of curvature can be determined at some position x.

$$\frac{1}{\rho} = \frac{d\theta}{ds} = \frac{P(L-x)}{EI}$$

Note that as the applied force increases the radius of curvature decreases.

106

APPENDIX B: SECOND ORDER MODEL

A second order model was simulated by using MatLab. The following is a derivation of the model used to describe torsional fiber dynamics.

For a mass, spring, dashpot system, the characteristic equation is given by equation 1.
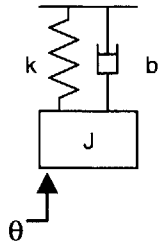
$$\tau = J\ddot{\theta} + 2\zeta\omega_n\dot{\theta} + k\theta \quad (1)$$

$$where \quad \tau = applied\ torque$$
$$J = moment\ of\ inertia$$
$$\zeta = damping\ factor$$
$$\omega_n = natural\ frequency$$
$$k = torsional\ stiffness$$
$$\theta = angular\ displacement$$

$$let \quad \theta_1 = \theta \quad \Rightarrow \quad \dot{\theta}_1 = \dot{\theta} = \theta_2 \quad (2)$$
$$\theta_2 = \dot{\theta} \quad \Rightarrow \quad \dot{\theta}_2 = \ddot{\theta} \quad (3)$$

Now substitute (2) and (3) into (1) :

$$\dot{\theta}_1 = \theta_2 \quad (4)$$
$$\tau = J\dot{\theta}_2 + 2\zeta\omega_n\theta_2 + k\theta_1 \quad (5)$$

Equations (4) and (5) can be written in state-space notation:

$$\begin{bmatrix} \dot{\theta}_1 \\ \dot{\theta}_2 \end{bmatrix} = \begin{bmatrix} 0 & 1 \\ -\dfrac{k}{J} & -\dfrac{2\zeta\omega_n}{J} \end{bmatrix} \begin{bmatrix} \theta_1 \\ \theta_2 \end{bmatrix} + \begin{bmatrix} 0 \\ \dfrac{1}{J} \end{bmatrix} \quad (6)$$

This linear system (6) was inputed into MatLab to simulate a torsional response. The next page contains the actual source script.

```
k=1.1144e-6;         %torsional stiffness
L=28.5;              %length in inches
Jyy=7.050e-6;        %moment of inertia
w=0.385;             %natural frequency (rad/s)
zeta=0.125;             %damping factor

%state space representation
a=[0 1; -k/Jyy -2*zeta*w];
b=[0; 1/Jyy];
c=[1 0; 0 0];
d=[0;0];

temp(1:239) =  0;       %temporary vector for plotting

xo=[10 0];          %initial conditions, 10 rad angular offset, 0
                    rad/sec %initial velocity
[y,x,t]=initial(a,b,c,d,xo);
plot(t,y(1:length(y),1),'r-', t, temp, 'k');
hold on

xo=[5 0];           %initial conditions, 5 radians offset, 0 rad/sec
                    %initial velocity
[y,x,t]=initial(a,b,c,d,xo);
plot(t,y(1:length(y),1),'r-', t, temp, 'k');

xo=[1 0];           %initial conditions, 1 radians offset, 0 rad/sec
                    %initial velocity
[y,x,t]=initial(a,b,c,d,xo);
plot(t,y(1:length(y),1),'r-', t, temp, 'k');
```

APPENDIX C: SENSITIVITY ANALYSIS

Since the equilibrium time constant is a function of the discrete length of fiber being untwisted, the spreadsheet in Table 3.11 evaluates the effect of position accuracy of the linear stage on the equilibrium time constant.

A second order torsional system has a natural frequency given by equation 1 and stiffness given by equation 2.
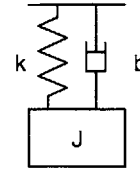
$$\omega_n = \frac{1}{T} = \sqrt{\frac{k}{J}} \qquad (1)$$

where T = period

k = torsional stiffness

J = mass moment of inertia

$$k = \frac{\tau}{\phi} = \frac{GI_p}{L} \qquad (2)$$

where τ = applied torque

ϕ = angle of rotation

G = shear modulus

I_p = polar moment of inertia

L = length

After substituting (2) into (1):

$$T = \frac{1}{\omega_n} = \sqrt{\frac{JL}{GI_p}} \qquad (3)$$

Next, differentiate (3) with respect to L:

$$\frac{dT}{dL} = \frac{1}{2}\sqrt{\frac{J}{GI_p L}} \qquad (4)$$

As shown in Table 3.11, equation 4 was evaluated for various lengths, L. For the case shown, dL was assumed to be 0.004in, an accuracy specification easily met by many linear stage manufacturers. The resulting change in the equilibrium time constant, dT, was considered negligible.

Table 3.11

Sensitivity Analysis							
Given:	dL	dL		Length		dT/dL	dT
	in	m		in	m	s/m	s
	0.004	0.0001016		24	0.6096	11.895	0.0012
				36	0.9144	9.712	0.0010
				48	1.2192	8.411	0.0009
				60	1.524	7.523	0.0008
				72	1.8288	6.868	0.0007
				78	1.9812	6.598	0.0007
				84	2.1336	6.358	0.0006
				90	2.286	6.143	0.0006